Validation of Odin/OSIRIS stratospheric NO2 profiles

Samuel M. Brohede, Craig S. Haley, Chris A. Mclinden, Christopher E. Sioris, Donal P. Murtagh, Svetlana V. Petelina, Edward J. Llewellyn, Ariane Bazureau, Florence Goutail, Cora E. Randall, et al.

Validation of Odin/OSIRIS stratospheric NO_2 profiles

Samuel M. Brohede,[1] Craig S. Haley,[2] Chris A. McLinden,[3] Christopher E. Sioris,[3,4] Donal P. Murtagh,[1] Svetlana V. Petelina,[4] Edward J. Llewellyn,[4] Ariane Bazureau,[5] Florence Goutail,[5] Cora E. Randall,[6] Jerry D. Lumpe,[7] Ghassan Taha,[8] Larry W. Thomasson,[9] and Larry L. Gordley[10]

Received 31 May 2006; revised 25 October 2006; accepted 20 November 2006; published 12 April 2007.

[1] This paper presents the validation study of stratospheric NO_2 profiles retrieved from Odin/OSIRIS measurements of limb-scattered sunlight (version 2.4). The Optical Spectrograph and Infrared Imager System (OSIRIS) NO_2 data set is compared to coincident solar occultation measurements by the Halogen Occultation Experiment (HALOE), Stratospheric Aerosol and Gas Experiment (SAGE) II, SAGE III, and Polar Ozone and Aerosol Measurement (POAM) III during the 2002–2004 period. Comparisons with seven Systeme d'Analyse par Observation Zenithal (SAOZ) balloon measurements are also presented. All comparisons show good agreement, with differences, both random and systematic, of less than 20% between 25 km and 35 km. Inconsistencies with SAGE III below 25 km are found to be caused primarily by diurnal effects from varying NO_2 concentrations along the SAGE III line-of-sight. On the basis of the differences, the OSIRIS random uncertainty is estimated to be 16% between 15 km and 25 km, 6% between 25 km and 35 km, and 9% between 35 km and 40 km. The estimated systematic uncertainty is about 22% between 15 and 25 km, 11–21% between 25 km and 35 km, and 11–31% between 35 km and 40 km. The uncertainties for AM (sunrise) profiles are generally largest and systematic deviations are found to be larger at equatorial latitudes. The results of this validation study show that the OSIRIS NO_2 profiles are well behaved, with reasonable uncertainty estimates between 15 km and 40 km. This unique NO_2 data set, with more than hemispheric coverage and high vertical resolution will be of particular interest for studies of nitrogen chemistry in the middle atmosphere, which is closely linked to ozone depletion.

Citation: Brohede, S. M., et al. (2007), Validation of Odin/OSIRIS stratospheric NO_2 profiles, *J. Geophys. Res.*, *112*, D07310, doi:10.1029/2006JD007586.

1. Introduction

[2] A number of satellite instruments have been launched recently that measure limb-scattered sunlight radiances with the goal of deriving vertical profiles of stratospheric minor species. These instruments include OSIRIS (Optical Spectrograph and Infrared Imager System) on the Odin satellite [*Warshaw et al.*, 1998; *Llewellyn et al.*, 2004] and SCIAMACHY (Scanning Imaging Absorption Spectrometer for Atmospheric Chartography) on Envisat [*Bovensmann et al.*, 1999]. GOMOS (Global Ozone Measurement by Occultation of Stars) on Envisat [*Bertaux et al.*, 1991] and SAGE (Stratospheric Aerosol and Gas Experiment) III on the Meteor-3M spacecraft [*McCormick et al.*, 1991] are primarily occultation instruments that also have limb-scatter measurement capabilities.

[3] The interest in the limb-scatter technique lies in a demand for atmospheric information with both global coverage and relatively high vertical resolution. The traditional sources of global stratospheric minor species information have largely been limited to either poor or no vertical information (nadir mapping instruments) or restricted spatial coverage (solar occultation instruments). The advantage of the limb-scatter technique is the provision of vertical profiles of stratospheric and mesospheric minor constituents with high vertical resolution (1–3 km) and near global coverage. A limitation to the technique is that only the measurements from the sunlit portion of each orbit can be utilized (i.e., daytime only). Passive emission instruments

[1]Department of Radio and Space Science, Chalmers University of Technology, Göteborg, Sweden.
[2]Centre for Research in Earth and Space Science, York University, Toronto, Ontario, Canada.
[3]Environment Canada, Toronto, Ontario, Canada.
[4]Department of Physics and Engineering Physics, University of Saskatchewan, Saskatoon, Saskatchewan, Canada.
[5]Service d'Aéronomie, Centre National de la Recherche Scientifique, Verrières le Buisson, France.
[6]Laboratory for Atmospheric and Space Physics and Department of Atmospheric and Oceanic Science, University of Colorado, Boulder, USA.
[7]Computational Physics Inc., Springfield, Virginia, USA.
[8]Science Systems and Applications Inc., Lanham, Maryland, USA.
[9]NASA Langley Research Center, Hampton, Virginia, USA.
[10]GATS Inc., Newport News, Virginia, USA.

0148-0227/07/2006JD007586

provide similar benefits as the limb-scatter technique and are not limited to measuring the sunlit atmosphere. The Michelson Interferometer for Passive Atmospheric Sounding (MIPAS) on Envisat [*Fischer and Oelhaf*, 1996] provides NO_2 profiles with a vertical resolution of about 4 km, but the retrievals require extensive non-LTE (Local Thermodynamic Equilibrium) calculations [*Funke et al.*, 2005].

[4] *Haley et al.* [2004] describe how NO_2 and O_3 can be successfully retrieved from OSIRIS limb-scatter measurements in the stratosphere using a combination of Differential Optical Absorption Spectroscopy (DOAS) [*Platt*, 1994] and Optimal Estimation (OE) [*Rodgers*, 2000]. OSIRIS provides a unique data set of NO_2 with a slightly more than hemispheric coverage and a vertical resolution of about 2 km between 15 and 40 km. A detailed error analysis was carried out by *Haley et al.* [2004] and the major sources of uncertainty were identified as pointing offset (tangent height registration), aerosols and cloud and concluded that the OSIRIS NO_2 profiles have an accuracy of 10% at the peak of the profiles.

[5] The purpose of this study is to validate the OSIRIS NO_2 product (version 2.4) and determine the systematic and random uncertainties. Four solar occultation instruments, HALOE (Halogen Occultation Experiment), POAM (Polar Ozone and Aerosol Measurement) III, SAGE (Stratospheric Aerosol and Gas Experiment) II, and SAGE III, are used for comparisons with coincident OSIRIS NO_2 measurements from 2002 to 2004. OSIRIS NO_2 profiles are also compared with SAOZ (Systeme d'Analyse par Observation Zenithale) balloon instrument measurements. Stratospheric NO_2 is an important species to measure because it is part of the NO_x chemistry, which is closely linked to ozone depletion; see section 2.

[6] Section 2 gives a brief description of nitrogen chemistry in the stratosphere and is followed by a brief overview of each instrument in section 3 and a short description of the OSIRIS retrieval process in section 4. Thereafter the validation process is described (section 5) and the results are presented (section 6). An analysis of the results is presented in section 7, followed by major conclusions and suggested future work in section 8.

2. Stratospheric NO_x Chemistry

[7] This section gives a brief introduction to stratospheric NO_x chemistry based on *Brasseur and Solomon* [1986] and references therein. The term NO_x refers to the sum of NO and NO_2 and is used due to the strong interaction between these species according to reactions (1) to (3) below. The term NO_y is reserved for all reactive nitrogen oxides, including NO, N_2O, NO_2, NO_3, N_2O_5, and HNO_3.

$$NO_2 + h\nu \rightarrow NO + O \quad (1)$$

$$NO_2 + O \rightarrow NO + O_2 \quad (2)$$

$$NO + O_3 \rightarrow NO_2 + O_2 \quad (3)$$

[8] The lifetime of NO_x is too short for it to cross the tropopause barrier in any significant amount, and the dominant sources of NO_x in the stratosphere are rather the more inert N_2O crossing the tropopause and to a small extent the polar winter descent of NO_y created by auroral processes.

[9] NO_x species are photochemically active, and the availability of solar radiation determines the relative abundance of NO and NO_2 as seen in reaction (1). During daytime conditions, the NO_x equilibrium is pushed toward NO. As the Sun sets the NO_2 concentration rapidly increases at the cost of NO (see Figure 1). In the nighttime chemistry an additional, but slower, processes take place, converting NO_x into NO_y:

$$NO_2 + O_3 \rightarrow NO_3 + O_2 \quad (4)$$

$$NO_2 + NO_3 + M \rightarrow N_2O_5 + M \quad (5)$$

The NO_3 and N_2O_5 are photolyzed during the daytime, creating NO_x again. The NO_3 concentration drops rapidly at sunrise, while N_2O_5 is more slowly photolyzed at stratospheric temperatures, which explains the positive NO_2 gradient during the day in Figure 1.

[10] NO_x chemistry is crucial to many stratospheric processes, including ozone depletion. Ozone (odd oxygen) is catalytically destroyed through the reaction cycle (2) and (3). In fact, photochemical loss of O_3 is dominated by NO_x between 25 km and 40 km altitude [*Dessler*, 2000]. In addition, NO_x is an important factor in the formation of reservoir species and in the creation of HNO_3-rich PSC (Polar Stratospheric Cloud) particles. The most important sink of stratospheric nitrogen inside the polar vortex is deposition of these particles to the troposphere (denitrification).

3. Instrument Descriptions

[11] Brief descriptions of the satellite orbit, instrument parameters, NO_2 retrieval method, and error estimation for each of the instruments are found below. An overview of the important parameters is found in Table 1. The viewing geometries of solar occultation and solar scattering instruments are illustrated in Figure 2.

3.1. OSIRIS Instrument

[12] The Optical Spectrograph and Infrared Imager System [*Llewellyn et al.*, 2004] is one of two instruments on board the Odin satellite [*Nordh et al.*, 2003]. Odin was launched in February 2001 into a 600 km circular Sun-synchronous near-terminator orbit with a 97.8° inclination and the ascending node at 1800 hours LST (Local Solar Time). Odin is a combination of astronomy and aeronomy missions with equal time disposition. OSIRIS is dedicated to aeronomy studies [*Murtagh et al.*, 2002] and a second instrument, the Submillimeter and Millimeter Radiometer (SMR) [*Frisk et al.*, 2003] carries out both aeronomy and astronomy studies. The instruments are coaligned and scan the limb of the atmosphere over a tangent height range 7 km to 70 km in approximately 85 seconds during normal stratospheric operations through controlled nodding of the satellite. Every 8th day in general and every 1–3 days

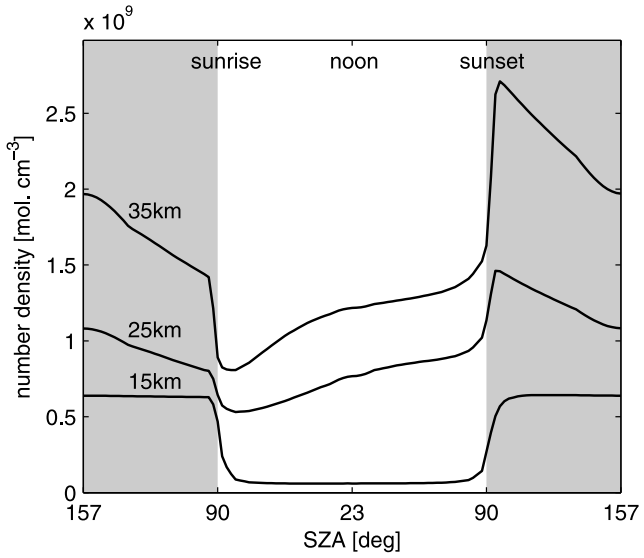

Figure 1. NO_2 concentrations as a function of solar zenith angle (SZA) and altitude based on simulations from the PRATMO chemical box model [*Prather*, 1992; *McLinden et al.*, 2000] for equatorial conditions (June, albedo = 0). The NO_2 concentration drops rapidly at sunrise due to photolyzation and increases similarly at sunset as NO_2 reforms from NO reacting with ozone (reaction (3)).

during the northern hemisphere summer, the scans are extended up to 100 km to cover the entire mesosphere.

[13] OSIRIS contains two optically independent components, the Optical Spectrograph (OS) and the Infrared Imager (IRI). The OS is a grating spectrometer that measures limb-scattered sunlight spectra in the spectral range 280 nm to 800 nm at a resolution of about 1 nm at tangent height intervals of roughly 2 km. The IRI is a three channel camera, imaging the atmospheric airglow emissions near 1.27 μm and 1.53 μm in a limb-viewing tomographic mode [*Degenstein et al.*, 2002]. The OS scattered sunlight measurements are used to provide vertical profiles of minor stratospheric constituents including O_3, NO_2, BrO, OClO, and aerosol, and are the focus of this study.

[14] The instantaneous field of view (FOV) of the OS is 1 km in the vertical and 40 km in the horizontal at the tangent point. When the nodding of the spacecraft and the varying exposure time of the OS ($\sim$0.01 s at 10 km increasing to $\sim$2 s at 50 km) are considered, the vertical resolution of the measured limb radiances is found to range from approximately 1 km at 10 km to 2 km at 50 km.

[15] The retrieval of NO_2 profiles from OSIRIS (version 2.4 data product) is discussed in section 4. Full global coverage of the OSIRIS NO_2 data is achieved around the equinoxes and hemispheric coverage is obtained during the rest of the year, as seen in Figure 3 (top). Data gaps are mainly due to Odin being in astronomy mode.

3.2. HALOE Instrument

[16] The Halogen Occultation Experiment [*Russell et al.*, 1993] was launched on the Upper Atmosphere Research Satellite (UARS) in September 1991 into a precessing 585 km altitude and 57° inclination orbit.

[17] HALOE is a solar occultation instrument with four radiometer channels and four dual radiometer/gas-filter correlation channels. It views the atmosphere in transmission with 15 sunrises and 15 sunsets per day. The occultation events occur in daily latitude bands, covering all latitudes between from 80°S and 80°N in approximately 36 days (see Figure 3). Vertical profiles of temperature, O_3, HCl, HF, CH_4, H_2O, NO, and NO_2 are retrieved from the measurements.

[18] The radiometer channels at 1015, 1510, and 1600 cm^{-1} are used for the NO_2 retrievals. Profiles are calculated with a modified onion-peeling approach using the High-Resolution Transmission (HITRAN) molecular absorption database (www.hitran.com). Interfering species include H_2O and CH_4 (both retrieved using separate channels) and O_2 (known). Extrapolated aerosol extinctions from the 1900 cm^{-1} vacuum-path channel are used to compensate for Mie scattering. NO_2 number densities are retrieved over the altitude range 10–50 km at a vertical resolution of 2 km and are reported at 300 m intervals. NO_2 gradients along the line of sight (LOS) are present due to the NO_x diurnal photochemistry discussed in section 2. This is compensated for in the HALOE retrievals by introducing a solar zenith angle (SZA) parameter in the forward model. The retrieved profile is then consistent with the atmospheric state at the subtangent point (STP); see Figure 2. The HALOE version 19 data product is used in this study.

Table 1. Summary of the Specifications of the Satellite Instruments in This Study[a]

Specification	OSIRIS	SAGE II	SAGE III	POAM III	HALOE
Geometry	solar scat.	solar occ.	solar/lunar occ.	solar occ.	solar occ.
Meas. type	full spectr.	7 channels	full spectr.	9 channels	4 rad.+4 gas corr.
Satellite	Odin	ERBS	Meteor-3M	SPOT-4	UARS
Launch	Feb 2001	Oct 1984	Dec 2001	Mar 1998	Sep 1991
Orbit type	sun synchr.	precessing	sun synchr.	sun synchr.	precessing
Eq. cross. time	18:00	-	09:00	22:30	-
NO_2 data					
Version	2.4	6.20	3	4	19
Alt. range, km	10–46	15–60	10–50	20–45	10–50
Sampling, km	2	0.5	0.5	1	0.3
Res.@30 km, km	2	1.5	2	1.5	2
Uncert.@30 km, %	10	15	10–15	5–10	10

[a]The resolution and uncertainty is generally a function of height for all instruments with a minimum at about 30 km. Note that the reported uncertainties are not entirely comparable since they are defined differently for each instrument.

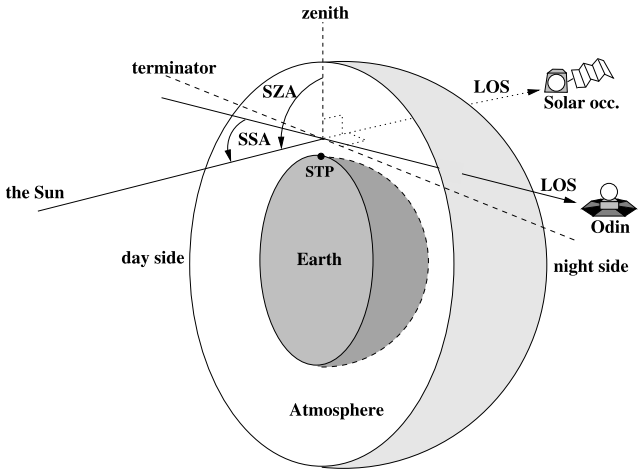

Figure 2. Viewing geometries of limb-scatter (OSIRIS) and solar occultation instruments. The OSIRIS viewing direction is usually close to parallel to the terminator, and the solar zenith angles (SZAs) and single scattering angles (SSAs) vary with season and geographical position. Solar occultation instruments always look perpendicular to the terminator. The figure is not to scale. LOS = line of sight, STP = subtangent point.

[19] According to *Gordley et al.* [1996], aerosol scattering dominates the extinction at low altitudes leading to poor NO_2 retrieval accuracy in the lower stratosphere (below 25 km). Other major error terms include random noise, pressure registration, interfering species, and spectral parameters. The total uncertainty, except aerosol extinction which is varying rapidly in time and space and thus difficult to quantify generally, is estimated to be about 10% at 30 km, increasing rapidly to 20% at 25 km and 40 km, and more than 60% at 15 km and 45 km. Infrequently, sunspots and Sun tracking errors can cause biased retrievals.

[20] Extensive correlative comparisons conducted by *Gordley et al.* [1996] on an older version of the HALOE NO_2 data (version 17) show good agreement (within 10–15%) in the middle stratosphere (25–35 km), but poor agreement below 25 km, especially for heavy aerosol conditions, where a low bias is evident. Between 35 km and 40 km a low bias of up to 5% was also indicated. *Randall et al.* [2002] compared the version 19 data product to NO_2 profiles from the Atmospheric Trace Molecule Spectroscopy experiment (ATMOS) [*Gunson*, 1996] and confirmed the good behavior of the HALOE data above 25 km (within 10%) and a low bias below 25 km of as much as 40%. The low bias between 35 km and 40 km was fixed in the new version.

3.3. POAM III Instrument

[21] The Polar Ozone and Aerosol Measurement III instrument [*Lucke et al.*, 1999] was launched on the SPOT (Satellite Probatoire d'Observation de la Terre) 4 satellite in March 1998 into a Sun-synchronous orbit (ascending node at 2230 hours LST) with an altitude of 833 km and a 98.7° inclination.

[22] POAM III is a solar occultation instrument with nine radiometer channels between 353 nm and 1018 nm. The instrument nominally makes 14 sunrise and 14 sunset measurements per day occurring in a latitude band from 55° to 71° in the northern hemisphere and from 63° and 88° in the southern hemisphere (see Figure 3). All POAM NH measurements are made during spacecraft sunrise but correspond to local sunset. SH observations are obtained during spacecraft sunset, and correspond to local sunrise from mid-April through mid-September and local sunset at other times. Vertical profiles of O_3, NO_2, and H_2O as well as aerosol extinction are measured.

[23] NO_2 is retrieved using Optimal Estimation and the differential absorption between two channels: 439.6 nm (on) and 442.2 nm (off) [*Lumpe et al.*, 2002]. NO_2 number densities are retrieved between 20 km and 45 km at 1 km intervals with a vertical resolution of 1.5–2.5 km below 40 km. Spherical symmetry is assumed and no SZA corrections are made. The POAM III version 4 data product is used in this study.

[24] The random error in the retrieved NO_2 profiles is estimated as 6% at 20 km, 3% at 30 km, and 7% at 40 km. The total error is estimated to be 5–10%, though conditions with dense PSCs are reported to induce large biases below 23 km.

[25] A validation study of version 3 of the POAM III data using HALOE data [*Randall et al.*, 2002] shows agreement to within 6% between 22 km and 33 km with no bias. Above 33 km a positive POAM III bias of up to 17% is indicated and is partly attributed to errors in the HALOE data. A hemispheric bias at 20 km (POAM III higher in the NH and lower in the SH by up to 30%) due in part to POAM III not accounting for SZA variations and individual instrument errors is also found. NO_2 values above 35 km are not significantly different in the version 4 data. Between

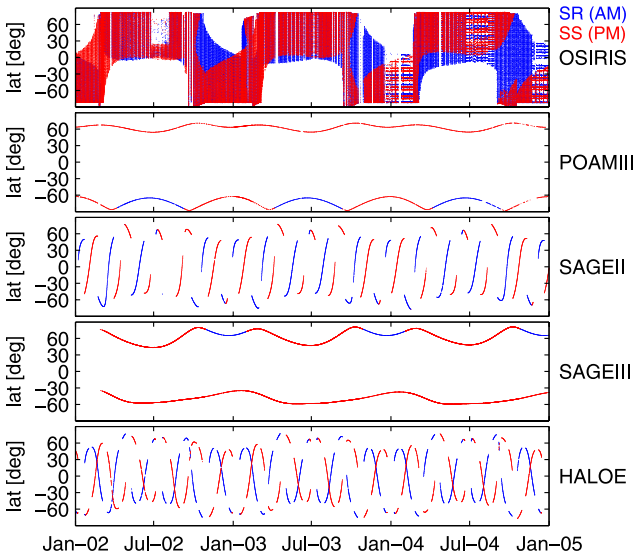

Figure 3. The latitudinal coverage of the satellite instruments in this study for sunrise (AM) and sunset (PM) measurements. POAM III and SAGE III provide measurements at small latitude bands around 60°, whereas the latitude coverage of SAGE II and HALOE varies from day to day in a repeatable pattern. OSIRIS gives near global coverage, which means all latitudes, near the equinoxes in addition to the summer hemisphere.

27 km and 33 km the values in version 4 are about 5–15% lower than in version 3. Below 25 km the version 4 data are significantly larger than in version 3, varying from 5% or less in the summer to up to 50% in the winter, where the NO_2 abundances are small (C. E. Randall et al., Comparison of solar occultation NO_2 measurements, manuscript in preparation, 2007).

3.4. SAGE II Instrument

[26] The Stratospheric Aerosol and Gas Experiment II instrument [*Mauldin et al.*, 1985] was launched on board the Earth Radiation Budget Satellite (ERBS) in October 1984 into a precessing orbit with an altitude of 610 km and a 56° inclination.

[27] SAGE II is a solar occultation photometer with a holographic grating and 7 channels between 385 nm and 1020 nm. The latitude coverage of SAGE II varies from day to day in a 1-year repeatable pattern, similar to HALOE, extending from approximately 70°S to 70°N (see Figure 3). SAGE II produces vertical profiles of aerosols, O_3, NO_2, and H_2O.

[28] Slant columns of NO_2 are calculated from the 448 nm and 453 nm channels using a differential technique [*Chu and McCormick*, 1989]. Vertical profiles are then retrieved between 15 km and 60 km using an onion peeling procedure, where the NO_2 slant columns are smoothed prior to peeling. The altitude sampling is 1 km and the vertical resolution for NO_2 is about 1.5 km below 39 km and 5 km above 39 km. As with POAM III, spherical symmetry is assumed and no SZA correction is applied. The SAGE II version 6.20 data product is used in this study, and compensates for the slight drift in the NO_2 channels after launch.

[29] The random error associated with the NO_2 retrievals between 27 km and 36 km is approximately 5%. The overall accuracy is estimated to be 15%, with the increase mostly due to NO_2 cross section uncertainties. Difficulties in separating NO_2, O_3, and aerosols below 23 km make measurements in that region highly uncertain.

[30] A validation study carried out by *Cunnold et al.* [1991] on an older version of data found the SAGE II NO_2 to be in agreement with balloon instruments to within 10% between 23 km and 32 km. Comparisons between SAGE II and HALOE by *Gordley et al.* [1996], also using an older version of data, indicated a significant bias in the SAGE II data due to aerosol contamination below 27 km, good agreement (10%) from 27 km to 33 km, and a negative bias of up to 25% above 33 km. *Taha et al.* [2004] analyzed the version 6.20 data product and found that the agreement with SAGE III NO_2 is within 5–9% in the altitude range 20–36 km.

3.5. SAGE III Instrument

[31] The Stratospheric Aerosol and Gas Experiment III instrument [*Thomason and Taha*, 2003] was launched on board the Russian Meteor-3M platform in December 2001 into a Sun-synchronous orbit with ascending node at 0900 hours LST. It is primarily designed to make solar and lunar occultation measurements but also has a limb-scatter measurement capability.

[32] The SAGE III instrument is a spectrometer covering wavelengths from 280 nm to 1040 nm with a 1–2 nm spectral resolution. An additional photodetector at 1550 nm is included. SAGE III provides 30 measurement events per day, 15 sunrises at high northern latitudes (45–80°N) and 15 sunsets at southern midlatitudes (25–60°S). All satellite sunrise measurements are at local sunset, while observations obtained during satellite sunset are also at local sunset except from mid-September through February, as seen in Figure 3. SAGE III measures O_3, NO_2, aerosol extinction, H_2O, NO_3 (lunar), OClO, cloud information, pressure, and temperature.

[33] Profiles of NO_2 are derived using a multiple linear regression (MLR) technique for two spectral channels (433–450 nm and 563–622 nm) [*NASA Langley Research Center*, 2002]. MLR simultaneously solves for O_3 and NO_2, which absorb significantly in both spectral regions. The uncertainty is estimated to be 10–15% (systematic) and 10–15% (random). Smoothing is applied to the NO_2 slant columns, giving an effective vertical resolution of about 2 km throughout the 10–50 km retrieval range (for other products the resolution is about 1 km). Number densities are reported at 0.5 km intervals and no SZA correction is applied. The SAGE III version 3 data product is used in this study.

[34] According to *Taha et al.* [2004], the agreement with SAGE II NO_2 is within 5–9% in the altitude range 20–36 km. Agreement with POAM III is within 10% above 22 km and with HALOE is within 5% between 25 km and 34 km. Large differences between SAGE III and HALOE below 25 km (up to 60%) are found and are likely due to SAGE III not accounting for SZA variations.

3.6. SAOZ Instrument

[35] The SAOZ (Systeme d'Analyse par Observation Zenithale) UV/visible spectrometer makes solar occultation measurements during the ascent/descent of the balloon and during sunset/sunrise from float. The balloon version of the SAOZ instrument is very similar to the one used for ground-based measurements of total ozone and NO_2 [*Pommereau and Goutail*, 1988]. Measurements are recorded between 290 nm and 640 nm with an average spectral resolution of 0.8 nm. Using an onion peeling method, SAOZ provides the vertical distribution of O_3, NO_2, and atmospheric extinction at a vertical resolution of 1.4 km with accuracies of better than 3% for O_3 and 10% for NO_2 [*Pommereau and Piquard*, 1994].

[36] The SAOZ NO_2 profiles are reported to agree to within 20% with POAM III from 23 km to 27 km, where SAOZ has a negative bias at 27 km and a positive positive bias at 23 km [*Randall et al.*, 2002]. At 20 km the mean difference is larger (50%). The SAOZ NO_2 data used in this study have not been corrected for diurnal variations along the line of sight.

4. OSIRIS NO_2 Retrievals

[37] A thorough description of the OSIRIS NO_2 retrievals can be found in the work of *Haley et al.* [2004]. Only a simplified description is given here.

4.1. DOAS Step

[38] Instead of retrieving NO_2 vertical profiles directly from the OSIRIS limb-scattered radiance measurements, an intermediate step is applied where effective column densities,

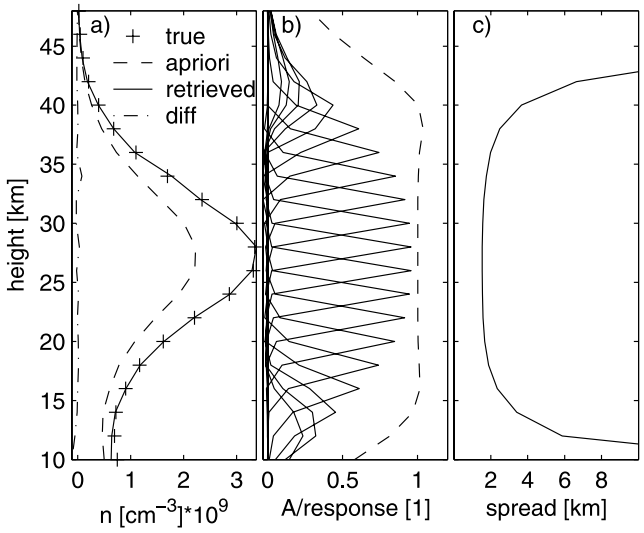

Figure 4. Typical NO_2 retrieval characteristics for a modeled, noise-free OSIRIS midlatitude limb scan (SZA = 85°, SSA = 90°). (a) The true, a priori (66% of the true), and retrieved profiles and the absolute difference between the true and retrieved profiles, (b) the averaging kernels (solid lines) and the measurement response (dashed line), and (c) the vertical resolution ("spread") are shown. High response (> 0.75) is usually found between 15 km and 40 km and the vertical resolution is about 2 km near 30 km.

ECD, (sometimes referred to as slant column densities) are calculated using Differential Optical Absorption Spectroscopy (DOAS) [*Platt*, 1994]. The DOAS step is performed to reduce the sensitivity to phenomena that vary slowly with wavelength such as aerosol (Mie) scattering.

[39] The wavelength region used for retrieving NO_2 is 435–451 nm, where the absorption is large compared with O_3 and strong Fraunhofer lines are avoided. An average of spectra measured between 46 km and 65 km tangent height from each limb scan is used as the reference spectrum, effectively reducing any Ring-effect and Fraunhofer signatures. O_3 and O_4 are included together with NO_2 in the nonlinear, least-squares fit, and the I_0-effect, wavelength shifts, and different trending in the reference and the measurement spectra (tilt-effect) are compensated for. The NO_2 absorption cross sections from *Vandaele et al.* [1998] are used.

4.2. Forward Model

[40] The pseudo-spherical multiple scattering radiative transfer model LIMBTRAN [*Griffoen and Oikarinen*, 2000] is used to invert ECD as a function of tangent height to number density as a function of height. Temperature and pressure information used in LIMBTRAN is from the European Centre for Medium-Range Weather Forecasts (ECMWF) analysis fields. Aerosol information is also included and consists of the stratospheric aerosol extinction climatology for 1999 from *Bauman et al.* [2003a, 2003b] and a Heney-Greenstein phase function (asymmetry parameter 0.7). The surface albedo is taken from *Koelemeijer et al.* [2003].

[41] LIMBTRAN assumes horizontal homogeneity within its vertical layers, and the retrieved profile is assigned to the location of the STP; see Figure 2. This can lead to errors in the retrieved profiles at times when horizontal variations in the true NO_2 distribution exists. Such variations exist in the NO_2 distribution near the terminator due to photochemistry and can affect the retrieved profiles, as will be discussed in section 4.5.

4.3. Inversion Process

[42] The inversion algorithm used to deduce vertical profiles of NO_2 from ECDs is Optimal Estimation (OE) or more specifically the nonlinear Maximum A Posteriori (MAP) estimator from *Rodgers* [2000], solved in a Gauss-Newton iterative manner. MAP is a Bayesian estimator giving the most probable solution based on the measurements and a priori information and the associated covariances. A positive constraint is applied to the retrievals by inverting in logarithm space. Profiles that have not converged after eight iterations or have converged with a high χ^2-value are discarded.

[43] A fixed retrieval grid is chosen, stretching from 10 to 46 km at 2 km intervals. It was found that the weighting functions can be calculated using only two wavelengths, single scattering, and no aerosol without significantly reducing accuracy. Good response (>0.75), i.e., low a priori contamination, is usually found between 15 km and 40 km and the resolution at 30 km is about 2 km, but this varies slightly from profile to profile depending on the measurement conditions.

[44] The NO_2 a priori information is taken from precalculated look-up tables constructed using a photochemical box model [*Prather*, 1992; *McLinden et al.*, 2000], initialized with input fields derived from climatology (O_3, T, aerosol surface area), three-dimensional model output (NO_2, NO_y), and tracer correlations (CH_4, HO_2, Cly, Bry). The a priori profile is chosen to be the nearest neighbor based on profiles tabulated bimonthly and every 2.5° in latitude and then interpolated in SZA to the value at the OSIRIS scan location. The covariance matrix of the a priori state is also required for the retrievals. NO_2 is assumed to follow a log-normal distribution, with standard deviations for the diagonal components of 60% and an exponential off-diagonal correlation length of 4 km. The measurement covariance matrix is a diagonal matrix with the variance of the propagated measurement noise in the diagonal. Measurements from different tangent altitudes are assumed uncorrelated. A sample NO_2 number density profile retrieved from a modeled noise-free OSIRIS limb scan is shown in Figure 4.

4.4. Error Budget

[45] The error estimation of the retrieved profiles is the crucial part of any inversion technique. As described by *Rodgers* [2000], four sources of error can be identified: (1) smoothing error, (2) retrieval noise, (3) forward model error, (4) forward model parameter error. The smoothing error and measurement noise components of the total retrieval error are easily calculated. However, the forward model and forward model parameter errors are more difficult to evaluate.

[46] The smoothing error arises due to the limited vertical resolution of the retrieval compared to the true atmospheric state. If the retrieved profile is said to represent a smoothed

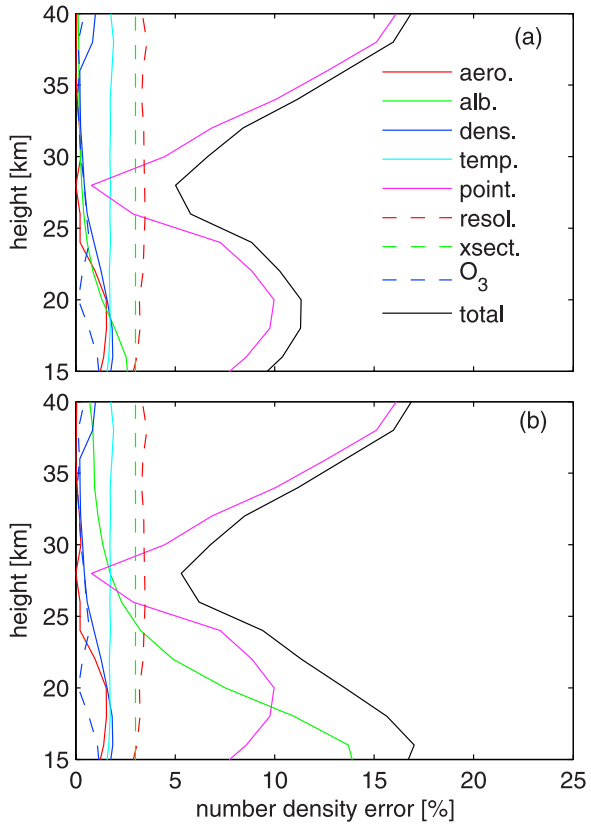

Figure 5. Forward model parameter errors for the OSIRIS NO_2 retrievals due to uncertainties in aerosol, surface albedo/cloud, neutral density, temperature, tangent height registration or pointing, spectral resolution, cross section, and ozone, given as 1σ, and the total forward model parameter error, given by the square root of the sum of the variances. Two scenarios are shown: (a) high-Sun (SZA = 60°, SSA = 90°) with cloud-free conditions and (b) high-Sun with clouds. Tangent height registration and albedo/cloud are the most significant errors and their influence increases below 27 km.

version on the true state, this error term can be ignored. Furthermore, when comparing retrieved profiles to profiles from another instrument with similar vertical resolution, the smoothing error becomes irrelevant. Henceforth, the OSIRIS smoothing error will not be included in the error budget for this validation study, where the vertical resolution of the various instruments only differs by a factor of two at most (see Table 1).

[47] Retrieval noise is the measurement noise propagated through the inversion process. This is a pure random error which is easily computed and verified.

[48] The forward model error is estimated by analyzing the impact of various approximations on the retrievals. The total forward model error for OSIRIS NO_2 retrievals was assessed by *Haley et al.* [2004] and found to be small (<5%), between 15 and 40 km, and generally independent of the measurement conditions. This type of error is mostly systematic. Note that no attempt was made to estimate the error introduced by the use of a pseudo-spherical forward model.

[49] The forward model parameter error concerns the uncertainty in input parameters to the forward model such as aerosol, neutral density, temperature, surface albedo, instrument spectral resolution, absorption cross sections, and the tangent height registration. *Haley et al.* [2004] studied these errors by treating them as independent error sources, each with an assumed uncertainty. The errors were estimated by performing perturbations of one standard deviation to a number of forward model parameters about a midlatitude atmosphere with surface albedo 0.3. In addition to the above error sources, the impact of cloud on the retrievals is estimated in a preliminary way by perturbing the surface albedo to a value of 1.0. Though crude, this gives a sense of the impact that can be expected when cloud is present in the measurements (below the FOV of the lowest measurement) but is not taken into account in the retrievals. An additional error that was not considered by *Haley et al.* [2004] was the impact of nonretrieved species (i.e., O_3), but this has now been included and has been found to be small (<1%). Assuming that each of the errors are independent and that vertical correlations can be ignored, the total forward model parameter error is given by the square root of the sum of the error variances of the individual errors. Note that no attempt was made to estimate the error introduced by the assumption of spherical homogeneity.

[50] Each of the forward model parameter error sources and the total are shown in Figure 5 for high-Sun (SZA = 60°) and for both cloudy and cloud-free conditions. Errors for low-Sun conditions (SZA $\approx$ 90°) are comparable to those of high-Sun cloud-free conditions and are not significantly sensitive to clouds. As the figure shows, tangent height registration (pointing) uncertainty is the largest source of error, potentially introducing errors of about 15% away from the peak. Clouds (albedo) can also have a large effect on the retrievals, leading to errors of about 15% below 20 km. Note that the tangent height registration uncertainty in the OS measurements is difficult to determine, but for this analysis it was estimated that the corrected tangent heights are accurate to 500 m (see section 4.6). The error due to cloud is also difficult to assess since the effective albedo of cloud depends on the characteristics of the cloud (e.g., thickness and patchiness) and on the solar conditions. The analysis here is essentially a worst-case scenario.

[51] If the three different error sources can be treated independently, the standard deviation of the total error is the square root of the sum of the three error variances. The total error is presented in Figure 6 for the two high-Sun cases mentioned above. As the figure shows, the estimated total error is about 10% at 30 km and increases to about 20% at 15 km and 40 km for cloud-free conditions. The error at 15 km increases to about 25% for cloudy conditions. These error levels are comparable to the occultation instruments.

4.5. Diurnal-Effect Error

[52] As noted above, one forward model parameter error source that was not evaluated by *Haley et al.* [2004] was the impact of the horizontal homogeneity assumption. When making near-terminator limb measurements related to photochemically active species with strong diurnal cycles, such as NO_2, the signal received at the sensor is an integration

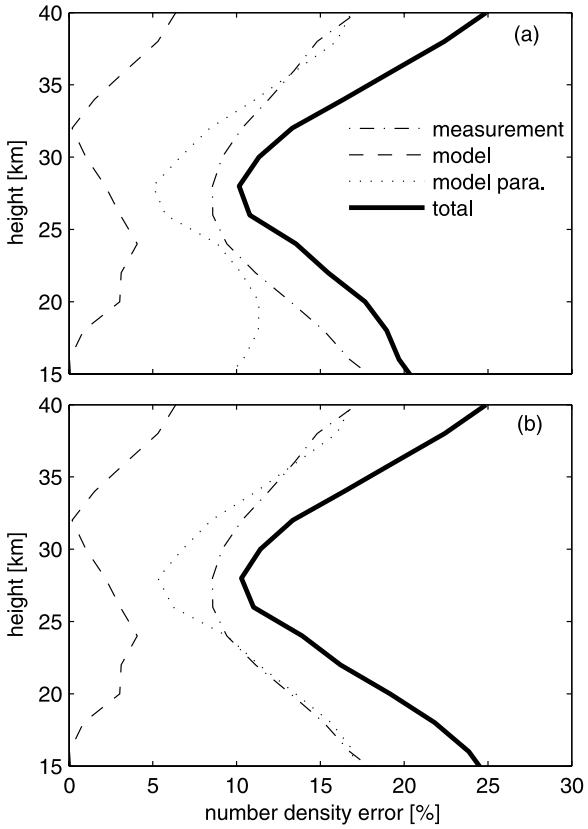

Figure 6. Error estimates (1σ) for OSIRIS NO_2 retrievals. Three main error sources are recognized; the measurement error (retrieval noise), the forward model error, and the forward model parameter error. The total error corresponds to the square root of the sum of the three variances. Two different scenarios are shown: (a) high-Sun (SZA = 60°, SSA = 90°) with cloud-free conditions and (b) high-Sun with clouds. Measurement error and forward model parameter error are the most significant and the total error adds up to 25% at 15 and 40 km at cloudy conditions and 10% at 27 km.

over a range of SZAs representing different atmospheric states with a potentially large variation in the number density of the target species. This so-called "diurnal effect" is not accounted for in the OSIRIS retrievals, where spherical homogeneity is assumed.

[53] The error introduced by not accounting for the diurnal effect will vary with the SZA and the angle between the incoming solar beam and the viewing direction (LOS) of the measurement, the so-called single scattering angle (SSA). For occultation measurements (with SZA = 90° and SSA = 0°) and limb-scatter measurements when SSA = 90°, the error is only related to variations along the incoming beam (see Figure 2). As the SSA deviates from 90° for limb-scatter measurements, variations along the LOS must also be considered. The OSIRIS SZA and SSA vary with latitude and season (see Figure 7) so that the SZA is always large in equatorial regions and small at high latitudes near the solstices. The SSA variation shows the largest deviations from 90° at the equator around the solstices and smaller deviations at high latitudes and around the equinoxes.

[54] Generally speaking, diurnal effect errors for limb-scatter instruments are expected to be largest below 25 km where the atmosphere is becoming optically thick and the signal is weighted toward the satellite (near) side of the LOS. At higher altitudes, errors from the far and near side will roughly cancel out because they have opposite signs. The diurnal effect errors are also linked to the magnitude of the diurnal NO_2 cycle, which is a function of altitude with stronger gradients at 15 km and 35 km than at 25 km, as seen in Figure 1.

[55] A model study conducted by *McLinden et al.* [2006] has shown that the overall diurnal effect errors do not exceed 10% above 25 km and reach a maximum at 14–18 km for OSIRIS viewing conditions (SZA = 60–90°, SSA = 60–120°). The magnitude and sign of the error below 25 km varies substantially with the viewing conditions as seen in Figure 8. For SZA = 90° and SSA = 90° (i.e., LOS exactly along the terminator) OSIRIS underestimates NO_2 by at most 25% for sunset conditions (PM) and slightly less at sunrise (AM). SSA > 90° gives further underestimation (up to 45% at 120°) while SSA < 90° introduces an overestimation of up to 20% at SSA = 60°. At SZA = 87.5°, the overestimation is about 25% at SSA = 60° but the corresponding underestimation at SSA = 120° is only about 20%. At SZA = 80° (and smaller), the diurnal effect errors are below 10% for all SSAs. Considering all of the OSIRIS NO_2 measurements over a 1-year period, *McLinden et al.* [2006] estimates that about 16% of all OSIRIS NO_2 profiles have diurnal effect errors of between 10% and 35% below 25 km, which is comparable to the size of the OSIRIS NO_2

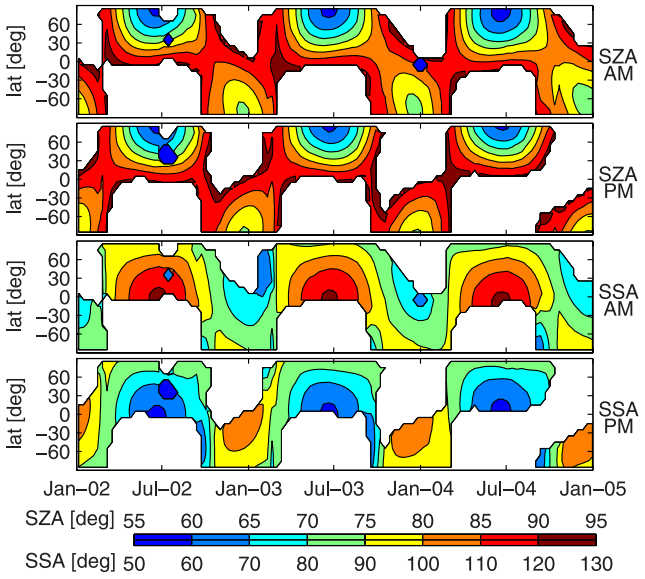

Figure 7. Solar zenith angle (SZA) and single scattering angle (SSA) for OSIRIS AM and PM measurements during the validation period 2002–2004. White regions indicate no OSIRIS measurements. The smallest SZAs are found in high-latitude summer conditions, whereas the SZA is close to 90° for all latitudes at the equinoxes. The SSA deviates furthest from 90° in the equatorial region in the northern latitude summer.

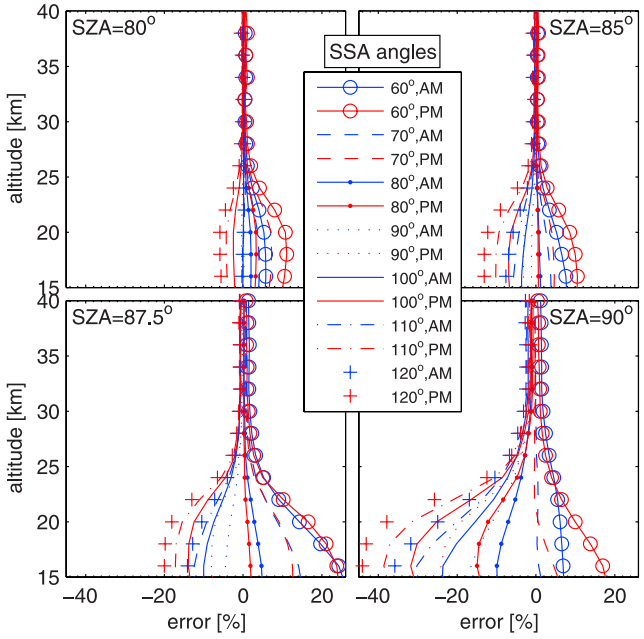

Figure 8. Estimated NO_2 limb-scatter diurnal errors for a range of typical OSIRIS SZA and SSA (the angles indicated in the legend) conditions based on equatorial conditions (June) with a ground albedo of 0.3. Diurnal errors arise due to inhomogeneous NO_2 concentrations along the scattering paths in conjunction with increasing optical depth at low tangent altitudes, see section 4.5. Generally, the diurnal error increases as the SZA approaches 90° and as the SSA departes from 90°. Above 25 km this error is insignificant regardless of the SZA and SSA.

total error estimate in this region (see Figure 6). The worst-case error, with extreme SSA, occurs at the solstices near the equator.

[56] The impact of the diurnal effect on solar occultation instruments also has to be considered in this validation study, except for HALOE which corrects for this. The error for occultation measurements has been assessed by applying the method of *McLinden et al.* [2006] to modeled occultation spectra. An OSIRIS-like instrument was assumed, with a retrieval approach using a DOAS spectral fit and a simple onion-peel inversion. The calculated errors for a few selected cases are found in Figure 9. The diurnal effect error for solar occultation instruments depends strongly on latitude and season and is generally consistent with the results of *Newchurch et al.* [1996]. A predicted systematic overestimation of about 20% for both AM and PM profiles is seen at 20 km, except for equatorial latitudes where the PM overestimation reaches 50%. The errors for December at 60°N and June at 60°S were not calculated because of limitations with the technique employed by the radiative transfer model (VECTOR) for varying the atmospheres along the LOS. Above 25 km the diurnal error is small (equatorial latitudes) or insignificant (high latitudes).

[57] In general, the diurnal effect error for occultation instruments is larger than that for OSIRIS except for equatorial latitudes at solstice where AM errors are larger and PM errors have similar magnitudes (and opposite signs). Unlike in limb-scatter, where most of the information comes from near the tangent point, the occultation measurements are sensitive to variations all along the LOS, with a weighting dependent on the contribution to the total optical depth (i.e., combination of path length and density). Hence whereas the limb-scatter measurements are affected by just the "local" diurnal error, the occultation error is affected by the variation in all layers above the tangent point, leading to the larger errors shown in Figure 9.

4.6. OSIRIS Pointing Offset Correction

[58] An approximate correction is used to account for a long-term Odin pointing drift (due to a satellite timing error) that has been identified, but is not accounted for in the OSIRIS version 2.4 NO_2 data product. A linear fit of the resulting retrieval altitude offset, z_{offset}, based on all scans up to 11 July 2004 (when the problem was corrected) gives

$$z_{offset} = t_{mjd} * \left(8.543 \cdot 10^{-4}\right) - 43.95; \quad (6)$$

where t_{mjd} is the modified Julian date (MJD) of the measurement. This offset value is added to the retrieval altitude grid. This correction approximately transforms the systematic pointing drift into a random pointing uncertainty of about 500 m, corresponding to a 10% uncertainty at 20 km, 5% at 30 km, and 15% at 40 km, as shown in Figure 5. Note that some additional error is introduced when correcting retrieved profiles, rather than correcting the

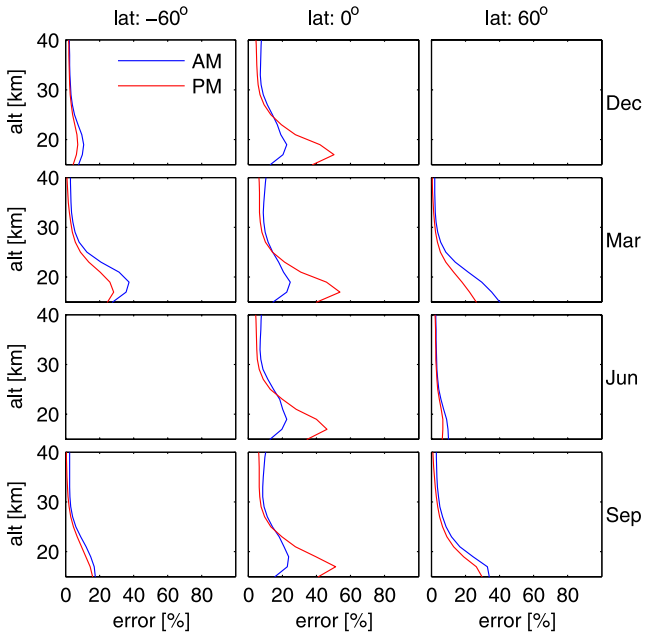

Figure 9. Estimated NO_2 diurnal errors for a typical occultation instrument for a selection of latitudes and months. Diurnal errors arise due to inhomogeneous NO_2 concentrations along the line of sight in conjunction with increasing optical depth at low tangent altitudes, see section 4.5. This error increases rapidly below 25 km and is significantly larger in PM at low latitudes. At high latitudes the diurnal error is largest around the equinoxes and AM values are slightly larger than at PM.

OSIRIS measurements prior to the retrieval process, due to nonlinearities.

5. Intercomparison Methodology

[59] When comparing limb-scattered sunlight measurements to solar occultation measurements, it is important to remember that the viewing geometries are quite different, as is seen in Figure 2, and can lead to differences even for measurements in which the STPs are colocated in time and space. Also, any deviation in the LST and location of the measurements can make the result difficult to interpret. This is particularly true for NO_2, which has a short atmospheric lifetime and strong variations between daytime and nighttime chemistry, enhanced by Odin's near-terminator orbit. An approach to compensate for different LSTs is described in section 5.2.

5.1. Finding Coincidences

[60] The validation period in this study stretches from January 2002 to December 2004, avoiding the first months of the Odin mission where there were satellite pointing problems, and excluding the more recent period where Odin's orbit has deviated significantly from the initial 1800 hour ascending node.

[61] A distance tolerance of 500 km is used in this study. This tolerance is loose enough to give a sufficient number of coincidences for an extensive statistical analysis, but tight enough to not impact significantly on the results of the analysis. The time tolerance is selected to be 2 hours UT. Owing to the diurnal variation of NO_2, a small time tolerance is needed, although 2 hours is not nearly small enough without SZA scaling (as described in section 5.2). Also, the different chemistry during sunrise (AM) and sunset (PM) necessitates that these categories are treated separately. For the SAOZ balloon comparisons, the distance tolerance was relaxed to 1000 km and the time tolerance was relaxed to 6 hours due to the small SAOZ data set. When more than one coincidence is found within the tolerances, the one which is closest in time (UT) is selected.

[62] All coincidences are further divided into three latitude bands: southern latitudes ($-90 \leq \text{lat} < -30$), equatorial latitudes ($-30 \leq \text{lat} \leq 30$), and northern latitudes ($30 < \text{lat} \leq 90$). This division is done to limit the impact of different atmospheric conditions on the comparisons, including cloudiness and tropopause height. In addition, the data is divided into four seasons: November–December–January (NDJ), February–March (FM), April–May–June–July–August (AMJJA), and September-October (SO). This division is logical when considering the OSIRIS latitude coverage over the year, where the northern hemisphere is covered between April and August, the southern hemisphere is covered from November to January, and full global coverage is achieved only close to the equinoxes (September/October and February/March) (see Figure 3).

[63] When interpreting the results, the altitudes have been divided into three regimes; high altitudes (35–40 km), midaltitudes (25–35 km), and low altitudes (15–25 km). The low-altitude regime is characterized by large uncertainties, including diurnal effect errors, SZA scaling biases, OS tangent height registration errors, cloud, aerosol, albedo, and a priori contamination. In the high-altitude regime, the signal to noise ratio for all instruments is generally declining and there is potential a priori contamination, depending on the retrieval technique. The midaltitude regime is presumed to contain the highest data quality for all instruments.

[64] The OSIRIS data are filtered based on measurement response (only >0.75 accepted) and vertical resolution (only <5 km accepted) to ensure that the a priori contamination is minimized. The other instrument data are filtered based on available data flags (any flagged data points are removed) and error estimate (any data points with an error estimate >100% are removed). To calculate differences, the OSIRIS data is interpolated to the altitude grid of the solar occultation instrument.

[65] To be entirely consistent, the vertical resolution of the instruments must be similar. If not, the resolution of one instrument must be transformed to the resolution of the other. This is omitted in this study since the resolution of all of the instruments is similar, only varying between 1 and 2 km (see Table 1), and resulting differences would only produce small errors that do not justify the effort of and potential errors introduced by the transformation.

5.2. SZA Scaling

[66] Owing to the sharp concentration gradients of NO_2 around sunset and sunrise (see Figure 1), even small deviations in SZA (or equivalently LST) of the coincident measurements can have a large impact on the results. Near the terminator, a SZA difference of a few degrees can lead to a change in the NO_2 concentration by a factor of 2 or 3 due to only photochemistry. Since the intention is to study differences in the general NO_2 field, meaningful comparisons can demand a very small SZA (or LST) tolerance, perhaps within a degree or a few minutes. Such strict requirements would reduce the number of coincidences dramatically, making a statistical analysis impossible.

[67] One solution to this problem is to use a photochemical model to scale the OSIRIS profile to the SZA of the other instrument, as is discussed by *Bracher et al.* [2005]. A tabulated photochemical box model (PRATMO) [*Prather*, 1992; *McLinden et al.*, 2000], driven by climatological ozone and temperatures, is used for this purpose. The look-up tables are given as a function of latitude (2.5° increments), time (2-week increments), altitude (2 km increments from 10 to 58 km), and SZA (up to 34 per day).

[68] The OSIRIS number density profiles at 90° SZA, $n_{OS}(90, z)$, are estimated by multiplying the profiles at the measured SZA, $n_{OS}(\theta_{OS}, z)$, by the model-based scaling factor s_θ;

$$n_{OS}(90,z) = \underbrace{\frac{n_{mod}(90,z)}{n_{mod}(\theta_{OS},z)}}_{s_\theta} n_{OS}(\theta_{OS},z), \tag{7}$$

where z is the altitude and n_{mod} are the model profiles obtained from the look-up tables. Points where s_θ is greater than 2 or less than 2/3 are discarded since the scaling is believed to lose accuracy at the extremes.

[69] Uncertainties in the SZA scaling for OSIRIS measurement conditions are shown in Figure 10 and have been estimated by repeating the calculation of s_θ after varying one of the assumed geophysical parameters by estimate of its uncertainty. The parameters considered (and their

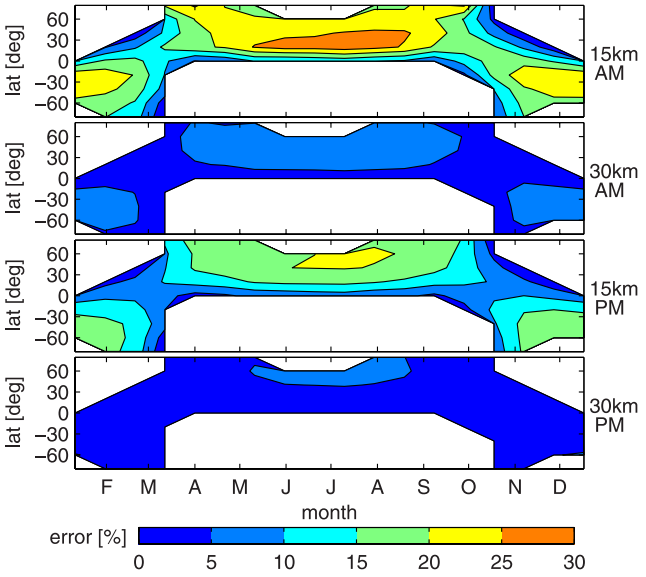

Figure 10. SZA scaling error for OSIRIS AM and PM measurements from estimated uncertainties in PRATMO parameters. The scaling error is insignificant at 30 km but substantial at 15 km with values up to 25% in midlatitude summer at AM.

uncertainties) are O_3 (30%), temperature (4 K), surface albedo (0.2), NOy (30%), Cly (30%), Bry (30%), and aerosol surface area (factor of 3). Additionally, uncertainties in the rates of NO + O_3 (30%) and NO_2 + hν (20%), two key rates controlling the NO_2 diurnal cycle, are considered. All individual uncertainties are added in quadrature to obtain an overall uncertainty estimate for s_θ. The uncertainties increase as the SZA departs from 90° (see Figure 7), as expected, and peak in the lower stratosphere (~15 km). The large uncertainties in this region are due to the assumed uncertainties in ozone and the rate of NO + O_3 (each contributing about equally) and are on par with the OSIRIS NO_2 profile retrieval uncertainty (~20%). Above 30 km the error is small (<5%) for all seasons and latitudes.

5.3. Statistical Analysis

[70] A statistical analysis is carried out when more than 12 coincidences are found within a latitude/season category (profiles and individual altitudes). The most relevant statistical parameter for studying systematic differences is the mean of the individual differences:

$$\bar{\Delta}(z) = \frac{1}{n}\sum_{i=1}^{n}\left[\frac{OS_i(z) - X_i(z)}{OS_i(z)}\right], \tag{8}$$

where n is the number of coincidences, X is the intercomparing instrument (i.e., POAM III, HALOE, or SAGE II/III), and z is the altitude. Random differences are studied through the standard deviation of the differences:

$$\Delta_\sigma(z) = \left\{\frac{1}{n-1}\sum_{i=1}^{n}\left[\left(\frac{OS_i(z) - X_i(z)}{OS_i(z)}\right) - \bar{\Delta}(z)\right]^2\right\}^{\frac{1}{2}}. \tag{9}$$

Within each category, systematic differences between the instruments appear as deviations in the mean of the differences from zero and random differences will contribute to the standard deviation. Scatterplots with fitted linear regression lines are complementary to these calculations, where systematic differences appear as deviations from the 1-1 line and random differences will contribute to the spread of the points, quantified by the r^2 value for the fit.

5.4. Random and Systematic Uncertainties

[71] The total uncertainty of an instrument includes both a systematic and a random part, sometimes referred to as accuracy and precision. A theoretical estimation of the total uncertainty of OSIRIS NO_2 is presented by *Haley et al.* [2004] (see also section 4.4) and found in Figure 6. A method of estimating the OSIRIS random and systematic uncertainties from the measured differences is described below.

[72] Systematic uncertainties in both instruments contribute to the observed mean differences, $\bar{\Delta}(z)$. In a perfect scenario where it could be assumed that the other instrument provides an unbiased measurement of the true atmospheric state, the OSIRIS NO_2 systematic uncertainty could be determined as the maximum of $|\bar{\Delta}(z)|$ found in all latitude/season categories. However, this is rarely the case and may never be the case since remote measurements can never perfectly retrieve the true state since the problem is constrained by both the measurement and retrieval technique. In addition, the comparison of two instruments that contain biases relative to the true state does not necessarily give insight into the systematic uncertainty, since similar biases will cancel. Comparing with an ensemble of instruments, like in this study, can help minimize this problem. An estimate of the OSIRIS systematic uncertainty is expressed as the range of max $|\bar{\Delta}(z)|$ from all four occultation comparisons. Note that the approximate combined diurnal error (from both the scattering and occultation instrument except for HALOE where only scattering is considered), is calculated for representative conditions (latitude, longitude, season, SZA, and SSA) of each latitude/season category and subtracted from $\bar{\Delta}$ when calculating the systematic uncertainties.

[73] The instrument random uncertainties, i.e., the repeatability of the measurements, are related to the measured random differences, Δ_σ, although the true values are smaller since real differences between the probed air masses and SZA scaling errors will contribute to Δ_σ. An upper limit of the random uncertainty can however be estimated from Δ_σ. If it is assumed that the instruments OS and X are independent with random uncertainties ϵ_{OS} and ϵ_X having standard deviations σ_{OS} and σ_X, respectively, then the standard deviation of the differences, Δ_σ equals $\sqrt{\sigma_{OS}^2 + \sigma_X^2}$. If both instruments are assumed to have equal uncertainty (i.e., $\sigma_{OS} = \sigma_X$), then ϵ_{OS} is given by

$$\epsilon_{OS}(z) = \sqrt{\frac{\Delta_\sigma^2(z)}{2}} \tag{10}$$

The theoretical random uncertainty (1σ) is about 10% at 30 km for all instruments, as seen in Table 1, which supports the assumption on which equation (10) is based. From each instrument, latitude/season category, and altitude

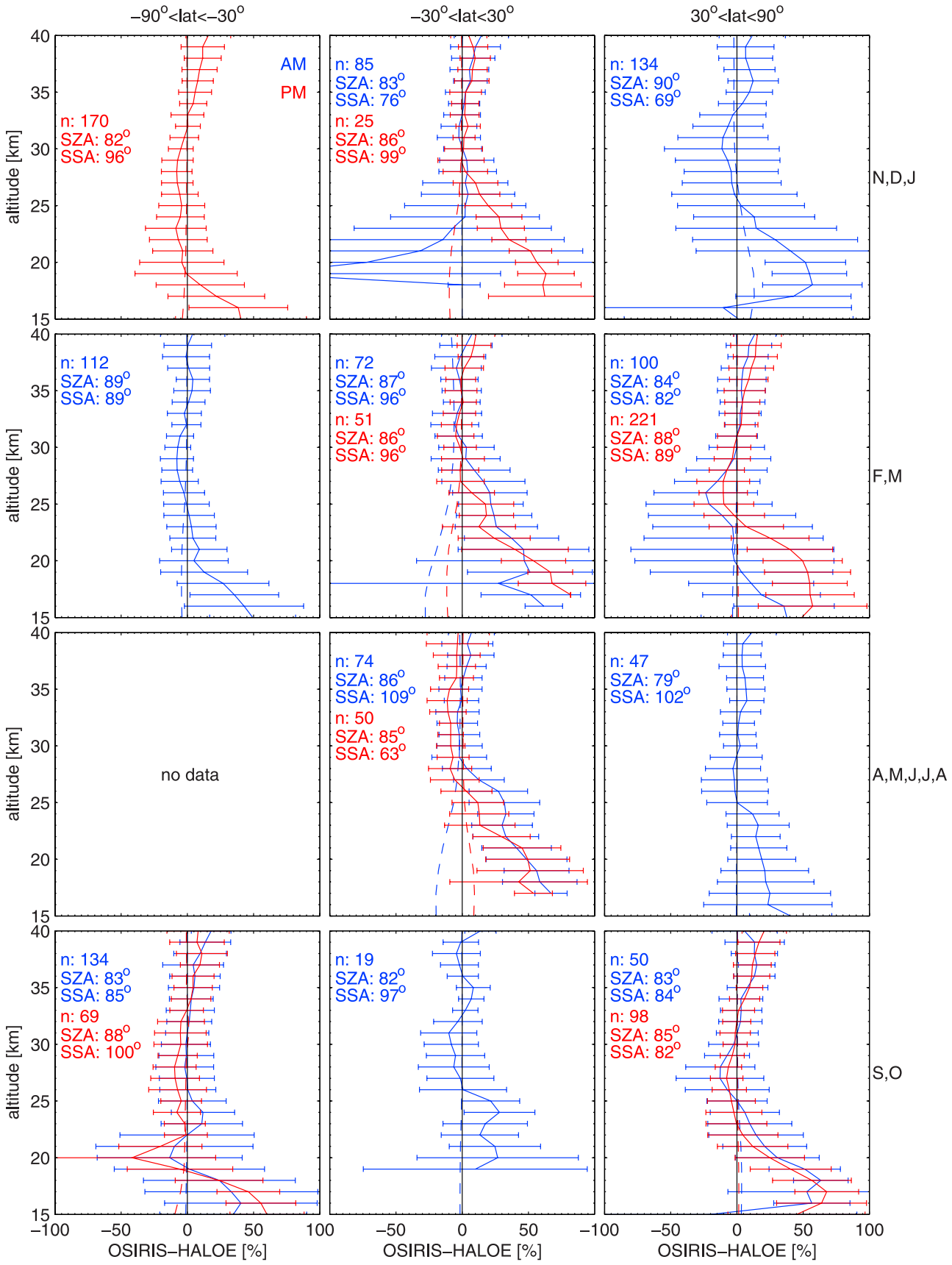
−90°<lat<−30°
−30°<lat<30°
30°<lat<90°
AM
PM
n: 170
SZA: 82°
SSA: 96°
n: 85
SZA: 83°
SSA: 76°
n: 25
SZA: 86°
SSA: 99°
n: 134
SZA: 90°
SSA: 69°
N,D,J
n: 112
SZA: 89°
SSA: 89°
n: 72
SZA: 87°
SSA: 96°
n: 51
SZA: 86°
SSA: 96°
n: 100
SZA: 84°
SSA: 82°
n: 221
SZA: 88°
SSA: 89°
F,M
no data
n: 74
SZA: 86°
SSA: 109°
n: 50
SZA: 85°
SSA: 63°
n: 47
SZA: 79°
SSA: 102°
A,M,J,J,A
n: 134
SZA: 83°
SSA: 85°
n: 69
SZA: 88°
SSA: 100°
n: 19
SZA: 82°
SSA: 97°
n: 50
SZA: 83°
SSA: 84°
n: 98
SZA: 85°
SSA: 82°
S,O
altitude [km]
OSIRIS−HALOE [%]

Figure 11

range, a value of ϵ_{OS} is calculated. The best estimate of the true instrument random uncertainty of OSIRIS is assumed to be the lowest value since this emanates from a category with the smallest atmospheric variation and the occultation instrument with lowest random uncertainty.

6. Results

[74] The intercomparison methodology presented in the previous section results in 7711 coincidences between OSIRIS and the other four satellite instruments. Figures 11 to 14 show the mean differences and the 1σ standard deviation of the mean differences for the four intercomparisons in each of the twelve categories, while Figure 15 shows scatter plots for all coincidences with each of the four instruments at five altitudes. Figure 16 shows additional comparisons between OSIRIS and four SAOZ balloon flights.

[75] Also shown in Figures 11 to 14 is the estimated diurnal effect error for each category. The diurnal effect error was simulated as discussed in section 4.5 and includes both the limb-scatter and the occultation components except for the HALOE comparisons, where only the limb-scatter component is shown since the HALOE retrievals include a diurnal effect correction. The error was simulated for the representative conditions in each category (average SZA, SSA, latitude, and day of year of the coincidences). The occultation component generally dominates this error in the conditions studied here.

[76] Detailed results from each instrument intercomparison are presented in the following sections and are summarized in Table 2. The results are given in three different altitude regions: high altitudes (35–40 km), midaltitudes (25–35 km), and low altitudes (15–25 km). Δ_σ values refer to one standard deviation (1σ). Results for individual years are not shown, but are consistent with the results from the full 3-year comparison period.

6.1. HALOE

[77] Altogether 830 sunrise (AM) and 687 sunset (PM) coincidences are found for OSIRIS and HALOE during the validation period. The results of these comparisons are shown in Figure 11. Coincidences are found in all latitude/season categories except for southern latitudes in AMJJA. The HALOE coincidences in the northern hemisphere in NDJ are the only coincidences for high latitudes around the winter solstice in the entire study.

[78] The Δ_σ for PM categories varies from 22–33% at low altitudes, 12–17% at midaltitudes, and 12–18% at high altitudes. The systematic differences, $\bar{\Delta}$, are within 70% at low altitudes, 11% at midaltitudes, and 20% at high altitudes, if equatorial categories, where the systematic difference increases rapidly below 30 km, are excluded. All categories show similar patterns, where OSIRIS is increasingly larger than HALOE below 20 km. The systematic differences below 25 km are not consistent with the estimated limb-scatter diurnal error.

[79] For AM profiles, Δ_σ varies from 24–60% at low altitudes, 13–35% at midaltitudes, and 14–20% at high altitudes, if the large values (>100%) at equatorial latitudes in NDJ are excluded. Northern latitudes in NDJ and equatorial latitudes in NDJ and SO tend to have the largest values. The systematic differences, $\bar{\Delta}$ are within 60% at low altitudes, 23% at midaltitudes, and 18% at high altitudes, again if the equatorial categories, where the difference is larger, are excluded. The OSIRIS NO_2 densities are significantly larger than HALOE at the lower altitudes for almost all categories. The equatorial region in NDJ in the AM is a clear exception, showing OSIRIS values that are smaller by more than 100%. The diurnal error estimates do not correlate with the AM systematic differences.

[80] The HALOE/OSIRIS scatter plots (Figure 15a) show very close fits to the 1-1 line (high r^2) at 25 km and 30 km, while OSIRIS shows larger NO_2 densities at 35 km and 40 km. The 15 km and 20 km plots show many outliers. The correlations are higher for PM comparisons at all altitudes.

[81] HALOE mean profiles and their corresponding standard deviations are not presented, but show very significant increases in NO_2 concentration and variability below 18 km, particularly for equatorial categories and in the AM. This pattern is not visible in the OSIRIS data set, the OSIRIS a priori data, or in the other instrument data sets except for SAGE II.

6.2. SAGE II

[82] For the OSIRIS and SAGE II data sets, 860 AM and 386 PM coincidences are found. The results of these comparisons are shown in Figure 12. The coincidences cover all latitude/season categories except southern latitudes in AMJJA and northern latitudes in NDJ.

[83] The PM Δ_σ varies from 17–86% at low altitudes, 9–17% at midaltitudes, and 15–22% at high altitudes, if equatorial latitudes and southern latitudes in FM, where the magnitudes reach several hundred percent at low altitudes, are excluded. The OSIRIS NO_2 densities are lower than SAGE II for most categories and the systematic differences ($\bar{\Delta}$) are within 26% at low altitudes, 17% at midaltitudes, and 31% at high altitudes, again if the equatorial latitudes and southern latitudes in FM are excluded. Southern latitudes have the smallest systematic differences and equatorial regions have the largest. The systematic differences are to some extent consistent with the estimated diurnal error in shape and sign, although the magnitude seems incorrect, especially for the equatorial regions.

[84] For AM coincidences, Δ_σ varies from 23–47% at low altitudes, 13–23% at midaltitudes, and 20–26% at high altitudes. The systematic differences, $\bar{\Delta}$, are within 56% at low altitudes, 21% at midaltitudes, and 25% at high altitudes, if the low-altitude range is constrained to 18–25 km, since values below 18 km deviate considerably. All

Figure 11. Results from OSIRIS and HALOE coincidences in 2002–2004, divided into 12 latitude/season categories and expressed as the mean (solid line) and 1σ standard deviation (error bars) of the differences. Sunrise (AM) and sunset profiles (PM) profiles are treated and plotted separately. The average solar zenith angle (SZA) and solar scattering angle (SSA) are given together with the number of coincidences (n) in each category. Estimated diurnal error biases (sum of occultation and limb-scatter) are plotted as dashed lines.

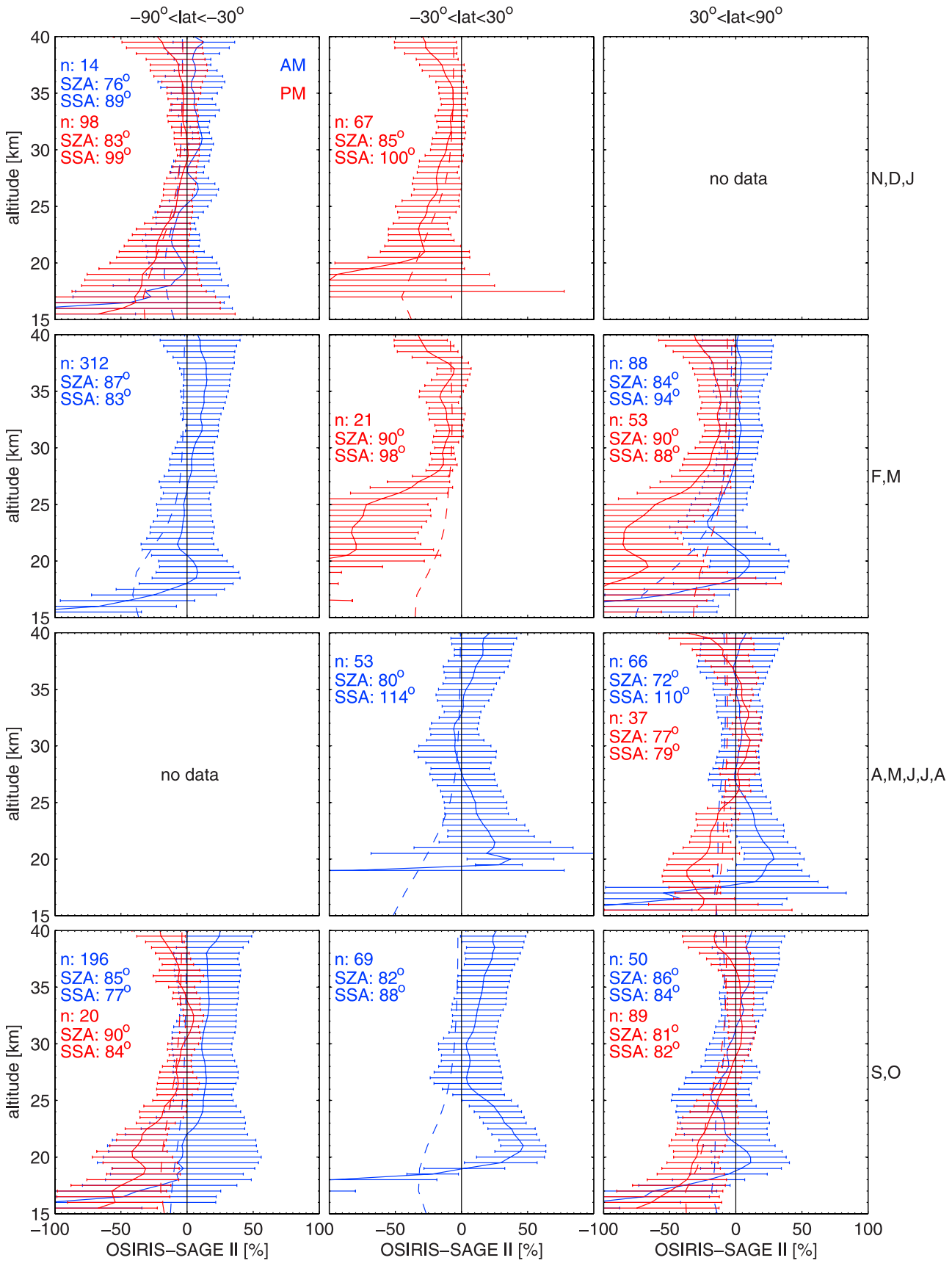

Figure 12. Same as Figure 11, but for SAGE II.

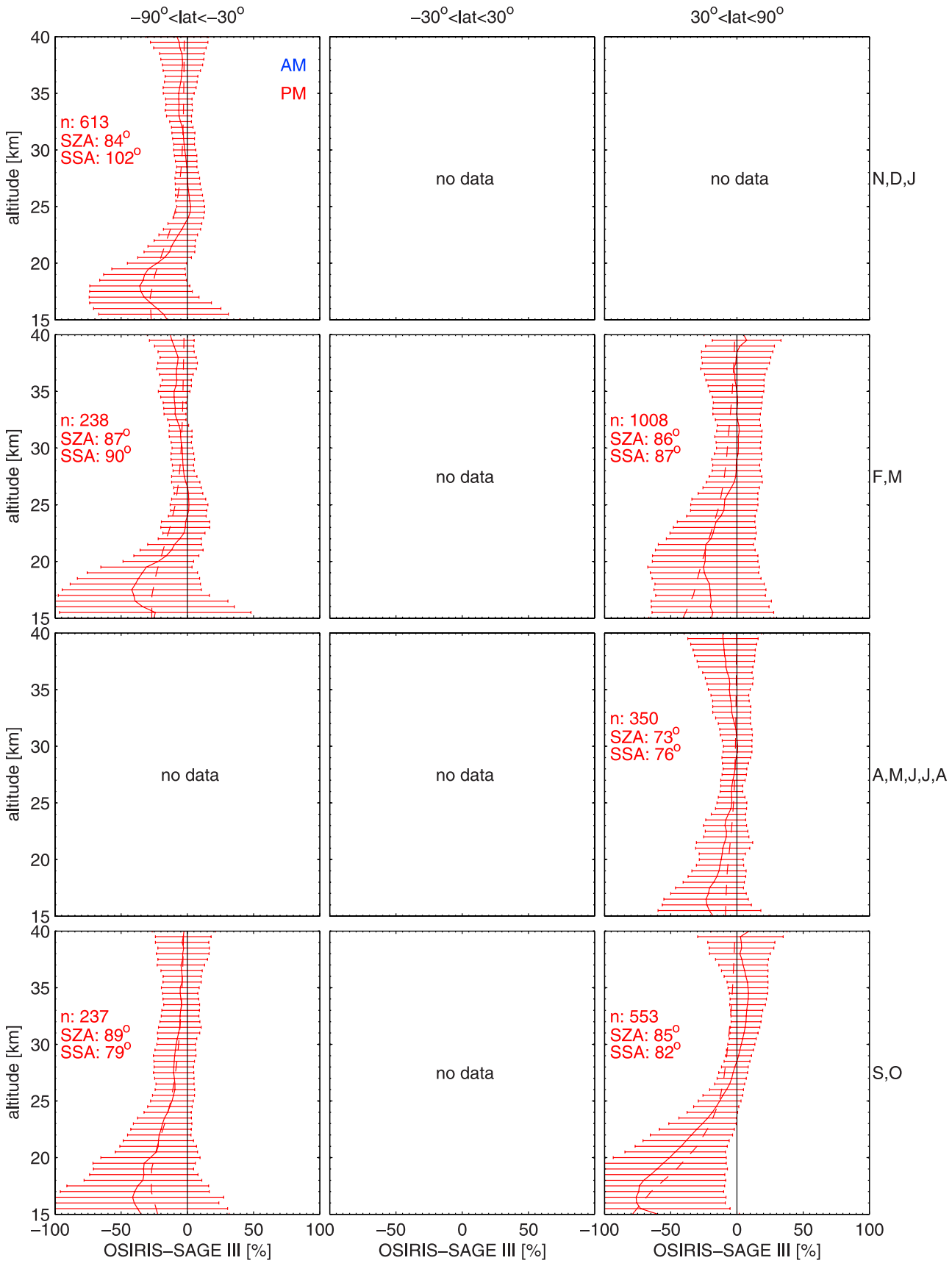

Figure 13. Same as Figure 11, but for SAGE III.

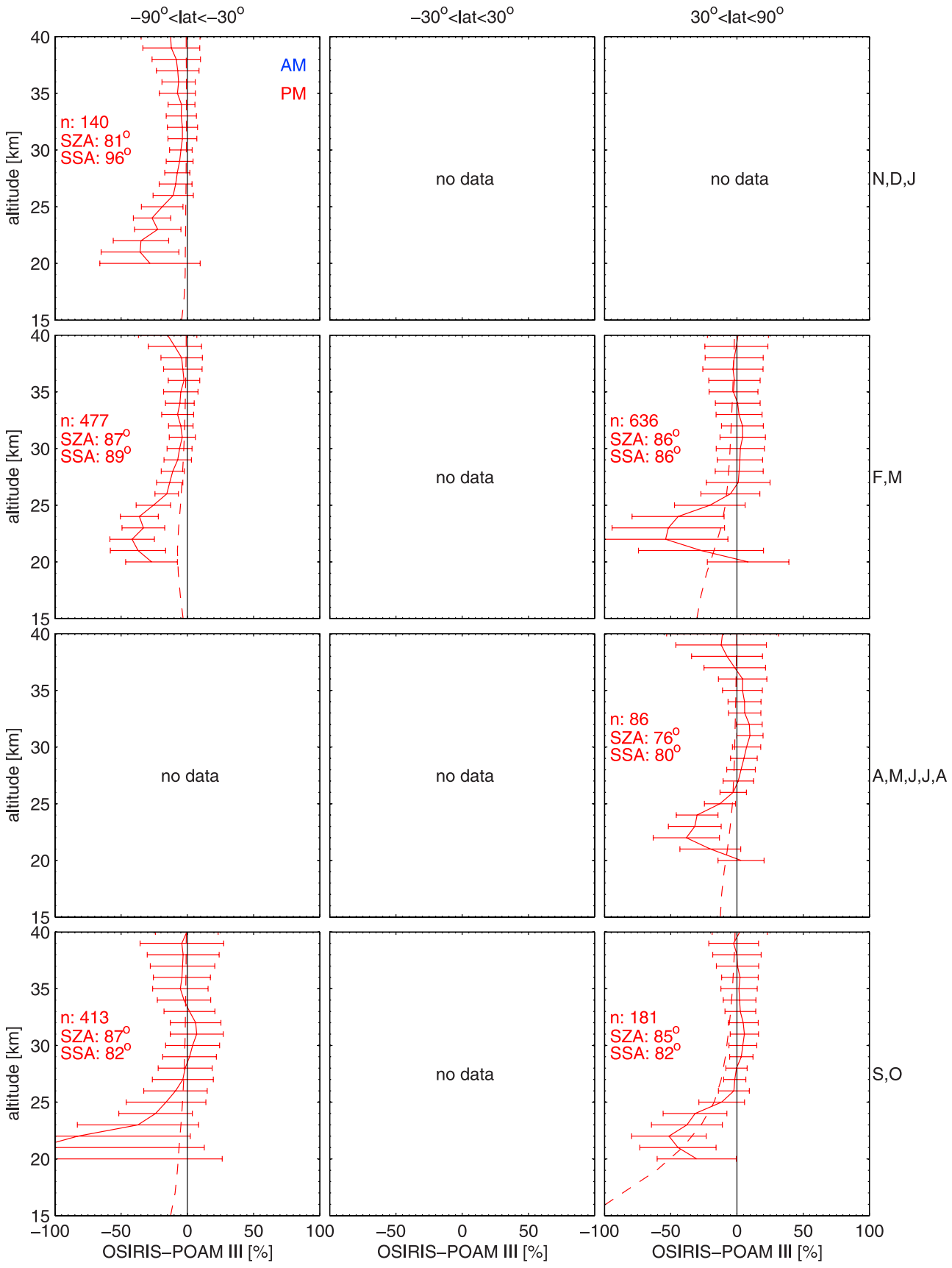

Figure 14. Same as Figure 11, but for POAM III.

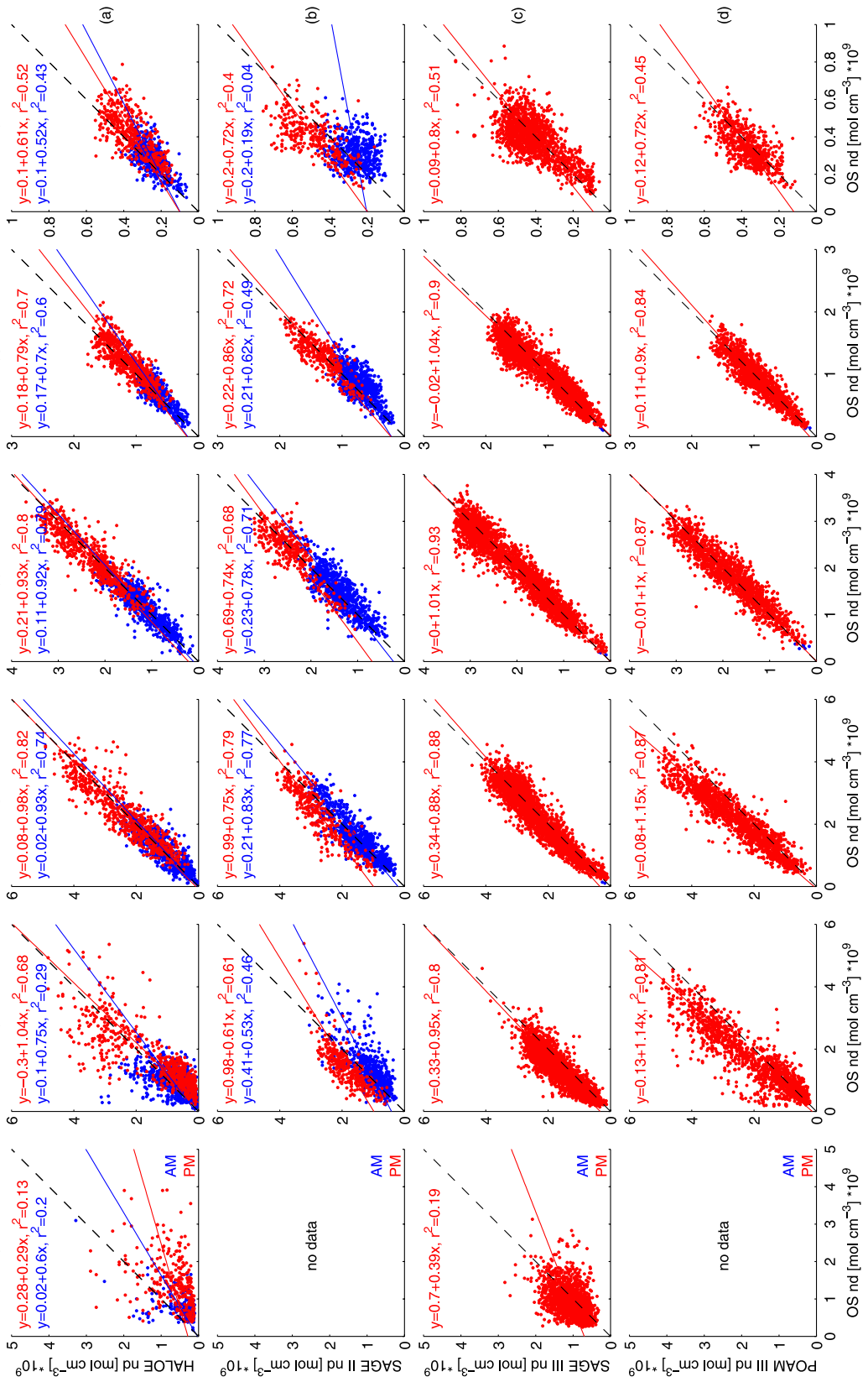

Figure 15. Scatterplots of OSIRIS versus the four solar occultation instruments ((a) = HALOE, (b) = SAGE II, (c) = SAGE III, (d) = POAM III) for all the coincidences in 2002–2004 at six altitudes. Sunrise (AM) and sunset profiles (PM) profiles are treated and plotted separately. Linear regression lines and their corresponding equations are included for each height The 1-1 line is given by the black dashed line.

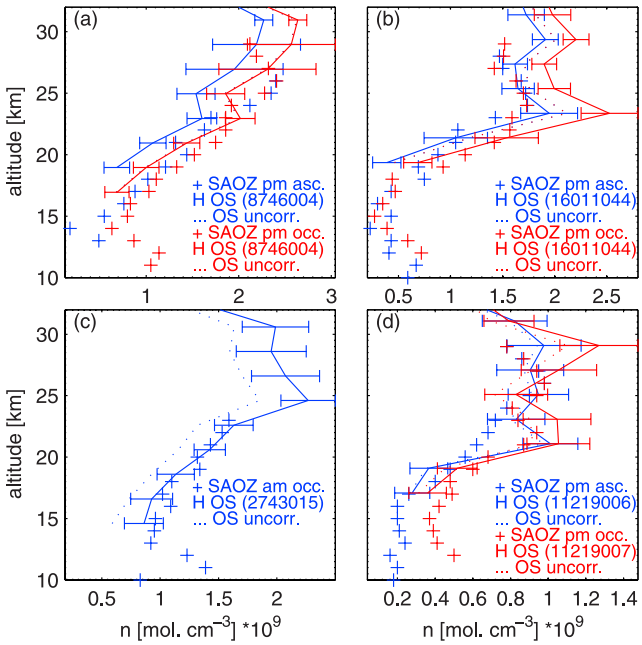

Figure 16. Comparisons of OSIRIS NO_2 profiles (solid and dotted lines) with results from four SAOZ flights (crosses). The closest coincidences in time and space for ascent (asc.) and occultation (occ.) are shown, with (solid lined with 1σ standard deviation uncertainties) and without (dotted lines) photochemical scaling of the OSIRIS profiles to the solar zenith angle of the respective SAOZ measurement. (a) NO_2 profiles retrieved from OSIRIS measurements on 1 October 2002 (scan:8745004, lat:39.2°N, lon:10°W, 1817 UT) and data from a SAOZ sonde launched at Aire sur l'Adour, France (PM ascent: lat:43.8°N, lon:0.1°W, 1700 UT, PM occultation: lat:43.7°N, lon:3.9°W, 1754 UT). (b) OSIRIS measurements on 31 January 2004 (scan:16011044, lat:24.6°S, lon:58.7°W, 2220 UT) and data from a SAOZ sonde launched at Bauru, Brazil (PM ascent: lat:22.4°S, lon:49°W, 2118 UT, PM occultation: lat:23.5°S, lon:53.4°W, 2206 UT). (c) OSIRIS measurements on 24 August 2001 (scan:2743015, lat:63.9°S, lon:29.5°W, 0508 UT) and data from a SAOZ sonde launched at Kiruna, Sweden (AM occultation: lat:67.9°N, lon:23.5°E, 0230 UT). (d) OSIRIS measurements on 16 March 2003 (scan:11218006, lat:66.1°N, lon:10.6°E, 16:12 UT, scan:11219007, lat:71.0°N, lon:4.9°E, 1614 UT) and data from a SAOZ sonde launched at Kiruna, Sweden (PM ascent: lat:67.5°N, lon:22.0°E, 1548 UT, PM occultation: lat:67.3°N, lon:14.3°E, 1654 UT).

categories show large negative systematic differences below 20 km, reaching up to several hundred percent at 15 km at equatorial latitudes. The estimated diurnal effect bias does not correlate with the measured AM bias at low altitudes.

[85] The SAGE II/OSIRIS scatterplots (Figure 15b) show close fits to the 1-1 line, with few extreme outliers, from 25 km to 35 km except for an OSIRIS high bias in the 35 km AM points. The fits at 20 km and 40 km are poor with a large number of outliers. PM comparisons show generally higher correlations, especially at the highest and lowest altitudes.

[86] The SAGE II mean profiles and their corresponding standard deviations are not presented but show a very significant increase in NO_2 concentration and variability below 20 km, especially for midlatitude categories and in the AM, similar to what is seen in the HALOE data.

[87] There seems to be a significant systematic difference between SAGE II SR and SS measurements at around 20 km for many categories, even though it is smaller than expected from the observed bias between SAGE II satellite SR and SS events [*Randall et al.*, 2005]. Note that for SAGE II and OSIRIS coincidences, local sunrise corresponds to satellite sunrise, except for a few cases in northern latitudes in NDJ.

6.3. SAGE III

[88] Owing to the latitude coverage of the Sun-synchronous orbits of SAGE III and OSIRIS, close coincidences in time and space only occur in southern and northern latitudes almost entirely at local sunset (PM). Altogether 3005 coincidences are found of which only six are in the AM, too few to make any statistical analysis. The coincidences appear in the northern and southern latitudes in all seasons except the winter solstices, as seen in Figure 13.

[89] All available latitude/season categories show similar patterns with a Δ_σ of 22–45% at low altitudes, 9–19% at midaltitudes, and 14–25% at high altitudes. Northern latitudes in FM stand out with significantly larger Δ_σ at middle and high altitudes. OSIRIS is systematically low by about 50%, peaking between 15 km and 20 km, which corresponds very well to the estimated diurnal errors in both magnitude and shape. If the estimated diurnal error is subtracted, the $\bar{\Delta}$ is within 21% at low altitudes, 12% at midaltitudes, and 11% at high altitudes.

[90] The SAGE III/OSIRIS scatterplots (Figure 15c) show generally good fits to the 1-1 line from 20 km to 35 km and a reasonable fit at 40 km, particularly at smaller concentrations. At 15 km, the fit is poor. The SAGE III mean profiles and corresponding standard deviations are not presented but are consistent with OSIRIS and do not show the low-altitude features seen in the HALOE and SAGE II data sets.

6.4. POAM III

[91] For OSIRIS and POAM III, close coincidences only occur in the southern and northern latitude regions, almost entirely at local sunset (PM). A total of 1943 coincidences are found of which only 10 are AM coincidences (again too few to make any statistical analysis). The categories around the winter solstices contain no coincidences due to the lack of OSIRIS data, as seen in Figure 14.

[92] The mean Δ_σ varies from 18–40% at low altitudes, 10–19% at midaltitudes, and 16–27% at high altitudes, if the southern latitude category in SO, which shows significantly larger Δ_σ, is excluded. Systematic differences, $\bar{\Delta}$, after the diurnal error is subtracted, are within 40% at low altitudes, 21% at midaltitudes, and 14% at high altitudes, again if the southern latitudes in SO are excluded. OSIRIS has systematically lower values by about 40% for southern latitudes and 50% for northern latitudes, peaking at about 22 km. The only exception is the southern latitudes in SO,

Table 2. Systematic and Random Differences (1σ) of OSIRIS Versus SAGE II, SAGE III, HALOE, and POAM III NO_2 Profiles (AM and PM) in Percent

	HALOE				SAGE II				SAGE III		POAM III	
Altitudes, km	AM rand.	PM rand.	AM syst.	PM syst.	AM rand.	PM rand.	AM syst.	PM syst.	PM rand.	PM syst.	PM rand.	PM syst.
35–40	14–20	12–18	18	20	20–26	15–22	25	31	14–25	11	16–27	14
25–35	13–35	12–17	23	11	13–23	9–17	21	17	9–19	12	10–19	21
15–25	24–60	22–33	60	70	23–47	17–86	56	26	22–45	22	18–40	40

where OSIRIS is lower by above 80%. The OSIRIS systematic low peak does not correspond to the estimated diurnal error.

[93] The scatterplots of POAM III/OSIRIS (Figure 15d) show a good fit to the 1-1 line only at 30 km and 35 km. Below 30 km, OSIRIS are clearly lower than POAM III, especially at high concentrations. At 20 km and 40 km the fit is fair due to many outlayers.

[94] The mean profiles of POAM III are not presented but show a typical sharp peak or double peak at 20 km, which roughly corresponds to the atmospheric NO_2 maximum. The OSIRIS mean NO_2 peak is smaller and much smoother. The sharp peak structure appears in almost all POAM III profiles and is not due to a few outliers in the data set. This behavior is not seen in any of the other instruments.

6.5. SAOZ

[95] Only four coincidences between OSIRIS and SAOZ balloon flights are found, even with the relaxed coincidence tolerances; hence no statistical analysis can be performed. However, as is shown in Figure 16, the four profiles generally agree to within the combined OSIRIS and SAOZ error bars (SAOZ error bars are not plotted for clarity) down to 15 km for most occasions except for the SAOZ PM occultation during the 31 January 2004 Bauru flight at altitudes above 20 km, where the OSIRIS SZA scaling correction appears to lead to an overestimate of the NO_2 concentrations, and for the PM ascent during the 1 October 2002 Aire sur l'Adour flight, where the SZA scaling appears to lead to an underestimation.

6.6. OSIRIS Uncertainties

[96] Estimated OSIRIS random and systematic uncertainties for AM and PM NO_2 profiles in the three altitude regimes are presented in Table 3. The values are estimated from the measured Δ_σ and $\bar{\Delta}$ of all latitude/season categories and instruments as described in section 5.4.

[97] SAGE II and HALOE have reported difficulties measuring NO_2 in the low-altitude regime, mainly due to problems with separating the NO_2 signal from other strong signals including aerosols and water vapor (see section 3.2 and 3.4), which makes these instruments less useful for estimating the OSIRIS uncertainty at low altitudes. The large and unexplained discrepancy between POAM III and OSIRIS below 25 km (which is traced to the POAM III data set since it does not appear in the other comparisons) makes also this data set inappropriate at low altitudes. Fortunately, the SAGE III data set appears to be well behaved down to 15 km (see Figure 13). Hence only SAGE III data have been used in the low-altitude regime. Furthermore, equatorial latitudes (for SAGE II and HALOE) are excluded from the calculations since they show major systematic uncertainties also at midaltitudes. SAGE II PM northern latitudes in FM and POAM III southern latitudes in SO have also been excluded due to strongly deviating results.

[98] As seen in Table 3, the OSIRIS random uncertainty for PM measurements is estimated to be 16% at low altitudes, 6% at midaltitudes, and 9% at high altitudes and is slightly higher for AM measurements. The systematic PM uncertainty is estimated to be about 22% at low altitudes, 11–21% at midaltitudes, and 11–31% at high altitudes, after correction for diurnal effect errors. The AM systematic uncertainty is estimated to be 21–23% at midaltitudes and 18–25% at high altitudes. Equatorial latitudes, which are excluded in the calculations, appear to have higher uncertainties; however, this is not quantified.

7. Discussion

[99] As is shown in Figure 6, the theoretical total uncertainty in the OSIRIS NO_2 profiles is smallest ($\sim$10%) near 30 km. At 15 km and 40 km, the uncertainty increases to 20–25%. The results of this study show a minimum in the random and systematic differences for all instruments near 30 km and increasing differences at high and low altitudes, which is consistent with the theoretical estimation.

[100] The agreement below 25 km is quite variable and generally poor, however, this is expected. At low altitudes, the signal to noise ratio of the NO_2 absorption signature in the measurements declines sharply due to the small NO_2 abundances. Furthermore, the atmosphere becomes optically thick (opaque) in the lower stratosphere at the wavelengths used by all of the instruments except HALOE. This tends to push the measurement focus toward the satellite side of the LOS since the contribution from the far side is decreased, increasing the diurnal effect errors and reducing the sensitivity of the instruments to NO_2 in the lower stratosphere. In addition, the SZA scaling error and many forward model parameter errors such as cloud, aerosol and albedo become

Table 3. Estimated Systematic and Random (1σ) Uncertainties of OSIRIS NO_2 AM and PM Profiles Based on the Mean and Standard Deviations of the Differences With SAGE II, SAGE III, HALOE, and POAM III

	Random		Systematic	
Altitudes, km	PM	AM	PM	AM
35–40	9%	10%	11–31%	18–25%
25–35	6%	9%	11–21%	21–23%
15–25[a]	16%	-	22%	-

[a]Only comparisons with SAGE III are used in this altitude regime.

important below 20 km. Decreasing signal to noise and possibly increasing pointing offset errors are the main reasons for the worse agreement at high altitudes (above 35 km). The generally larger random uncertainties for AM profiles are likely related to the small AM NO_2 abundances (as compared to PM profiles).

[101] One thing to notice is that solar scattering and solar occultation techniques probe different air masses even if a measurement corresponds to the very same STP. Solar occultation instruments sample NO_2 along the solar beam, but the scattering instruments sample partly along the solar beam and partly along the instrument LOS (considering single scattering only, the multiple scattering component of the signal further complicates the picture). If the atmospheric NO_2 concentration is truly spherically homogeneous, as is assumed in the retrievals, this is not a problem. The true concentration can, however, vary horizontally, due to photochemistry and near the vortex edge, for example. The two different techniques, then, should not be expected to give exactly the same result even if the measurements are perfect with no noise or other errors. However, a large number of coincidences will tend to minimize this problem (in terms of a systematic effect).

[102] As was mentioned in section 5.3, random uncertainties in the various instruments will contribute to the observed Δ_σ. In a perfect scenario, where no other sources of error contribute and where both instrument have exactly equal uncertainties, the real OSIRIS NO_2 random uncertainty can be calculated. However, coincidence issues, random errors in the SZA scaling factor, OSIRIS pointing error, vertical/horizontal resolution differences, a priori contamination and any other nonretrieved parameters that can affect the retrievals in a random way within each category (i.e., cloud, aerosols, and albedo) will potentially lead to an overestimation of the random uncertainty. This is particularly true at low altitudes where the various contributions are generally most significant. Nevertheless, the estimated OSIRIS random uncertainty, as seen in Table 3, is consistent with the theoretical measurement error (Figure 6). This indicates that the potential overestimation is small (or that the theoretical measurement error is underestimated).

[103] OSIRIS SZA scaling errors could possibly explain some of the differences at altitudes below 25 km. From Figure 10, the error should be more pronounced in the summer solstice periods (i.e., NH in AMJJA and SH in NDJ) and less significant around the time of the equinoxes where the SZA is close to 90° (i.e., in FM and SO). In addition, AM profiles should be more affected. However, nothing in the results indicates that the SZA scaling is a major random error source. To confirm this, the comparisons were repeated while limiting the included OSIRIS measurements to those where the SZA was within 2° of 90°, thus making the SZA scaling factor negligible). Very similar patterns to those presented in the previous section were found, indicating that indeed the SZA scaling is not a major source of the observed differences.

[104] OSIRIS uses a climatological albedo in the NO_2 retrievals (assuming no clouds) which may introduce systematic errors of up to 15% at 15 km for high Sun conditions (SZA = 60°) in the presence of clouds, as seen in Figure 5, and small errors in low Sun conditions. The largest albedo errors (due to the presence of clouds) are then expected in the summer high latitudes. However, this pattern is not evident in the comparisons.

[105] Systematic and random differences may also be related to aerosols since OSIRIS has some sensitivity to the accuracy of the aerosol climatology used in the retrievals, and the other instruments (HALOE, SAGE II, and POAM III in particular) are known to have significant aerosol-related errors at low altitudes. This error should generally be largest in the equatorial region. Peaks at the lowest altitudes in the NO_2 mean profiles exist in the HALOE and SAGE II data but not in SAGE III and POAM III data. Such peaks also do not exist in the OSIRIS NO_2 profiles or the aerosol climatology used in the OSIRIS retrievals. These peaks in the lower altitudes are likely the cause of the large mean difference values and are likely due to, for example, the LOS passing directly through clouds. This should mostly occur in the tropical region where tropical convective clouds may extend into the lower stratosphere or in regions of polar stratospheric clouds.

[106] The ad hoc OSIRIS tangent height registration correction that has been applied to the NO_2 data could also be a source of the systematic differences at low altitudes since in this region a simple shift of the retrieved profiles in height can lead to large errors due to a priori contamination and nonlinearities in the retrievals. However, this would be expected to impact the comparisons with all instruments. The remaining OSIRIS pointing uncertainty of approximately 500 m is expected to introduce random errors of about 10% at 20 km, 5% at 30 km, and 15% at 40 km and is likely contributing to the observed standard deviations of the differences.

[107] The combined diurnal effect error (both occultation and scattering) explains most of the systematic differences between OSIRIS and SAGE III at low altitudes. Both the magnitude and the shape of the error is consistent with the differences in all of the categories. In the POAM III and SAGE II PM data the diurnal effect error may explain part of the observed differences at low altitudes. For the other comparisons the contribution of the diurnal error to the observed systematic differences at low altitudes remains unclear. The approximation of the combined diurnal error for representative conditions (as plotted in the result Figures 11 to 14) are believed to be more accurate for POAM III and SAGE III where the latitudes are restricted to a small latitude band. A more accurate approach is to simulate the diurnal error for each profile within a category, not just for a representative case. However, this involves extensive computer runs and is left for future studies.

[108] It is difficult to make any quantitative assessment of the OSIRIS data quality based on the SAOZ comparisons due to the small number of coincidences and since the distance and time criteria are large. However, it can be said that the results are consistent and that no obvious biases exist.

[109] The assumption of independence made in the calculation of the random uncertainties can be questioned since the same NO_2 cross sections, and atmospheric parameters such as temperature and pressure are sometimes used in the retrievals for the various instruments. However, since the viewing geometries and the retrieval techniques are fundamentally different (except for OSIRIS and POAM III, which both use OE) the measurements should be largely independent.

Furthermore, HALOE measurements are made in the infrared and are consistent with OSIRIS measurements in the visible.

8. Conclusions

[110] Stratospheric NO_2 profiles retrieved from OSIRIS limb-scatter measurements (version 2.4) have been compared with NO_2 profiles measured with the HALOE, SAGE II, SAGE III, and POAM III satellite occultation instruments. All together 7711 coincidences were found within 2 hours and 500 km tolerances, between 1 January 2002 and 31 December 2004. Comparisons were also made with the SAOZ balloon occultation instrument.

[111] The agreement between OSIRIS and the satellite instruments is excellent between 25 km and 35 km, where both the random and systematic differences are within 20%. This is true for all instruments, seasons, and latitudes, except for a few exceptional cases. From 35 km to 40 km, the agreement is within 30%. The systematic agreement is slightly better for high latitudes than for equatorial latitudes. Below 25 km only OSIRIS and SAGE III are consistent. Model simulations indicate that the systematic difference between OSIRIS and SAGE III at low altitudes to a large extent can be attributed to diurnal effects in the SAGE III measurements from varying NO_2 concentrations along the line of sight. The SAOZ comparisons, though limited in number, show good agreement with OSIRIS down to 15 km, which further indicates high-quality OSIRIS measurements throughout the entire altitude range (15–40 km).

[112] On the basis of on the measured differences, the OSIRIS random uncertainty (~precision) is estimated to be 9% from 35 km to 40 km, 6% from 25 km to 35 km, and 16% from 15 km to 25 km. The systematic uncertainty (~accuracy) is estimated to be 11–31% from 35 km to 40 km, 11–21% from 25 km to 35 km, and around 22% from 15 km to 25 km. The AM uncertainties are found to be slightly higher than the PM uncertainties. These results correspond well to the theoretical uncertainties.

[113] Given the results of this validation study, the OSIRIS NO_2 profiles are well behaved, with reasonable uncertainty estimates throughout the entire retrieval range of 15–40 km. This unique NO_2 data set, with more than hemispheric coverage and high vertical resolution will be of particular interest for studies of nitrogen chemistry in the middle atmosphere, which is closely linked to ozone depletion.

[114] **Acknowledgments.** This work is supported by the Natural Sciences and Engineering Research Council (Canada), the Canadian Space Agency, the Swedish National Space Board, and Chalmers University of Technology. Odin is a Swedish-led satellite project, funded jointly by Sweden (SNSB), Canada (CSA), Finland (Tekes), and France (CNES). POAM III analyses are supported by the NASA data buy program and by the NASA Solar Occultation Satellite Science Team program. The SAGE II, SAGE III, and POAM III data were obtained from the NASA Langley Research Center EOSDIS Distributed Active Archive Center. Thanks also goes to the HALOE and SAOZ teams for providing data and support.

References

Bauman, J. J., P. B. Russell, M. A. Geller, and P. Hamill (2003a), A stratospheric aerosol climatology from SAGE II and CLAES measurements: 1. Methodology, *J. Geophys. Res.*, *108*(D13), 4382, doi:10.1029/2002JD002992.

Bauman, J. J., P. B. Russell, M. A. Geller, and P. Hamill (2003b), A stratospheric aerosol climatology from SAGE II and CLAES measurements: 2. Results and comparisons, 1984–1999, *J. Geophys. Res.*, *108*(D13), 4383, doi:10.1029/2002JD002993.

Bertaux, J., G. Mégie, T. Widemann, E. Chassefiè, R. Pellinen, E. Kyrölä, S. Korpela, and P. Simon (1991), Monitoring of ozone trend by stellar occultations: The GOMOS instrument, *Adv. Space. Res.*, *11*, 237–242.

Bovensmann, H., J. P. Burrows, M. Buchwitz, J. Frerick, S. Noël, V. V. Rozanov, K. V. Chance, and A. P. H. Goede (1999), SCIAMACHY: Mission objectives and measurement modes, *J. Atmos. Sci.*, *56*, 127–150.

Bracher, A., M. Sinnhuber, A. Rozanov, and J. P. Burrows (2005), Using a photochemical model for the validation of NO_2 satellite measurements at different solar zenith angles, *Atmos. Chem. Phys.*, *5*, 393–408.

Brasseur, G., and S. Solomon (1986), *Aeronomy of the Middle Atmosphere*, 2nd ed., Springer, New York.

Chu, W. P., and M. P. McCormick (1989), SAGE II inversion algorithm, *J. Geophys. Res.*, *94*, 8339–8351.

Cunnold, D. M., et al. (1991), Validation of SAGE II NO_2 measurements, *J. Geophys. Res.*, *96*, 12,913–12,925.

Degenstein, D. A., E. J. Llewellyn, and N. D. Lloyd (2002), Volume emission rate tomography from a satellite platform, *Appl. Opt.*, *42*(8), 1441–1450.

Dessler, A. E. (2000), *The Chemistry and Physics of Stratospheric Ozone*, Elsevier, New York.

Fischer, H., and H. Oelhaf (1996), Remote sensing of vertical profiles of atmospheric trace constituents with MIPAS limb emission spectrometers, *Appl. Opt.*, *35*, 2787–2796.

Frisk, U., et al. (2003), The Odin satellite I. Radiometer design and test, *Astron. Astrophys.*, *402*, L27–L34, doi:10.1051/0004-6361:20030335.

Funke, B., et al. (2005), Retrieval of stratospheric NOx from 5.3 and 6.2 Mm nonlocal thermodynamic equilibrium emissions measured by Michelson Interferometer for Passive Atmospheric Sounding (MIPAS) on Envisat, *J. Geophys. Res.*, *110*, D09302, doi:10.1029/2004JD005225.

Gordley, L. L., et al. (1996), Validation of nitric oxide and nitrogen dioxide measurements made by the halogen occulation experiment for uars platform, *J. Geophys. Res.*, *101*, 10,241–10,266.

Griffoen, E., and L. Oikarinen (2000), LIMBTRAN: A pseudo three-dimensional radiative transfer model for the limb-viewing imager OSIRIS on the Odin satellite, *J. Geophys. Res.*, *105*, 29,717–29,730.

Gunson, M. R. (1996), The atmospheric trace molecule spectroscopy (ATMOS) experiment: Deployment on the ATLAS space shuttle missions, *Geophys. Res. Lett.*, *23*, 2333–2336.

Haley, C. S., et al. (2004), Retrievals of stratospheric O_3 and NO_2 profiles from Odin Optical Spectrograph and InfraRed Imager System (OSIRIS) limb-scattered sunlight measurements, *J. Geophys. Res.*, *109*, D16303, doi:10.1029/2004JD004588.

Koelemeijer, R. B. A., J. F. de Haan, and P. Stammes (2003), A database of spectral surface reflectivity in the range 335–772 nm derived from 5.5 years of GOME observations, *J. Geophys. Res.*, *108*(D2), 4070, doi:10.1029/2002JD002429.

Llewellyn, E. J., et al. (2004), The OSIRIS instrument on the Odin spacecraft, *Can. J. Phys.*, *82*, 411–422.

Lucke, R. L., et al. (1999), The polar ozone and aerosol measurement (POAM) III instrument and early validation results, *J. Geophys. Res.*, *104*, 18,785–18,799.

Lumpe, J. D., R. M. Bevilacqua, K. W. Hoppel, and C. E. Randall (2002), POAM III retrieval algorithm and error analysis, *J. Geophys. Res.*, *107*(D21), 4575, doi:10.1029/2002JD002137.

Mauldin, L. E., III, N. H. Zaun, M. P. McCormick, J. H. Guy, and W. R. Vaughn (1985), Stratospheric aerosol and gas experiment II instrument: A functional description, *Opt. Eng.*, *34*, 307–312.

McCormick, M. P., W. P. Chu, J. M. Zawodny, L. E. Mauldin III, and L. R. McMaster (1991), Stratospheric aerosol and gas experiment III (SAGE III) aerosol and trace gas measurements for earth observing system (EOS), *Proc. SPIE Int. Soc. Opt. Eng.*, *1491*, 125–141.

McLinden, C. A., S. Olsen, B. Hannegan, O. Wild, M. J. Prather, and J. Sundet (2000), Stratospheric ozone in 3-D models: A simple chemistry and the cross-tropopause flux, *J. Geophys. Res.*, *105*, 14,653–14,665.

McLinden, C. A., C. S. Haley, and C. E. Sioris (2006), Diurnal effects in limb scatter observations, *J. Geophys. Res.*, *111*, D14302, doi:10.1029/2005JD006628.

Murtagh, D., et al. (2002), An overview of the Odin atmospheric mission, *Can. J. Phys.*, *80*, 309–319.

NASA Langley Research Center (2002), SAGE III algorithm theoretical basis document (ATBD) solar and lunar algorithm, *Tech. Rep. LaRC-475-00-109, Version 2.1*, Hampton, Va.

Newchurch, M. J., et al. (1996), Stratospheric NO and NO_2 abundances from atmos solar-occultation measurements, *J. Geophys. Res.*, *23*, 2373–2376.

Nordh, H. L., et al. (2003), The Odin orbital observatory, *Astron. Astrophys.*, *402*, L21–L25, doi:10.1051/0004-6361:20030334.

Platt, U. (1994), Differential optical absorption spectroscopy (DOAS), in *Air Monitoring by Spectroscopic Techiques*, edited by M. Sigrist, pp. 27–84, John Wiley, Hoboken, N. J.

Pommereau, J. P., and F. Goutail (1988), O_3 and NO_2 ground-based measurements by visible spectrometry during arctic winter and spring 1988, *Geophys. Res. Lett.*, *15*, 891–894.

Pommereau, J. P., and J. Piquard (1994), Ozone, nitrogen dioxide and aerosol vertical distribution by UV-visible solar occultation from balloons, *Geophys. Res. Lett.*, *21*, 1227–1230.

Prather, M. J. (1992), Catastrophic loss of stratospheric ozone in dense volcanic clouds, *J. Geophys. Res.*, *97*, 10,187–10,191.

Randall, C. E., et al. (2002), Validation of POAM III NO_2 measurements, *J. Geophys. Res.*, *107*(D20), 4432, doi:10.1029/2001JD001520.

Randall, C. E., et al. (2005), Update on the SOSST Unified Data Base and Occultation Intercomparisons, paper presented at Solar Occultation Satellite Science Team Meeting, NASA, Washington, D. C.

Rodgers, C. D. (2000), *Inverse Methods for Atmospheric Sounding: Theory and Practise*, 1st ed., World Sci., Tokyo.

Russell, J. M., et al. (1993), The halogen occultation experiment, *J. Geophys. Res.*, *98*, 10,777–10,797.

Taha, G., L. W. Thomason, C. R. Trepte, and W. P. Chu (2004), Validation of SAGE III data products version 3.0, paper presented at Quadrennial Ozone Symposium, Int. Ozone Comm., Kos, Greece. (Available at http://ioc.atmos.uiuc.edu)

Thomason, L. W., and G. Taha (2003), SAGE III aerosol extinction measurements: Initial results, *Geophys. Res. Lett.*, *30*(12), 1631, doi:10.1029/2003GL017317.

Vandaele, A., et al. (1998), Measurements of the NO_2 absorption cross-section from 42000 cm^{-1} to 10000 cm^{-1} (238–1000 nm) at 220 K and 294 K, *J. Quant. Spectrosc. Radiat. Transfer*, *59*, 171–184.

Warshaw, G., D. Desaulniers, and D. Degenstein (1998), Optical design and performance of the Odin UV/visible spectrograph and infrared imager instrument, paper presented at 10th Annual Conference on Small Satellites, Am. Inst. of Aeronaut. and Astronaut., Logan, Utah. (Available at http://www.smallsat.org/proceedings)

A. Bazureau and F. Goutail, Service d'Aéronomie-Centre National de la Recherche Scientifique, Reduit de Verrières-BP3, 91371 Verrières le Buisson Cedex, France. (ariane.bazureau@aerov.jussieu.fr; florence.goutail@aerov.jussieu.fr)

S. M. Brohede and D. Murtagh, Department of Radio and Space Science, Chalmers University of Technology, SE-412 96 Göteborg, Sweden. (samuel.brohede@chalmers.se; donal.murtagh@chalmers.se)

L. Gordley, GATS Inc., 11864 Canon Boulevard, Suite 101, Newport News, VA 23606, USA. (larry@gats-inc.com)

C. Haley, Centre for Research in Earth and Space Science, York University, 4700 Keele Street, Toronto, Ontario, M3J 1P3, Canada. (cshaley@yorku.ca)

J. Lumpe, Computational Physics Inc., 1650 38th Street, Suite 105, Boulder, CO 80301, USA. (lumpe@cpi.com)

C. McLinden and C. Sioris, Environment Canada, 4905 Dufferin Street, Toronto, Ontario, M3H 5T4, Canada. (chris.mclinden@ec.gc.ca; csioris@cfa.harvard.edu)

S. Petelina and E. Llewellyn, Department of Physics and Engineering Physics, 116 Science Place, University of Saskatchewan, Saskatoon, Saskatchewan, S7N 5E2, Canada. (svetlana@osirus.usask.ca; edward.llewellyn@usask.ca)

C. Randall, Laboratory for Atmospheric and Space Physics, University of Colorado, Boulder, CO 80309-0392, USA. (cora.randall@lasp.colorado.edu)

G. Taha, Science Systems and Applications Inc., 10210 Greenbelt Road, Suite 400, Lanham, MD 20706, USA. (ghassan_taha@ssaihq.com)

L. Thomasson, Science Directorate, NASA Langley Research Center, Mail Stop 475, Hampton, VA 23681-2199, USA. (l.w.thomasson@nasa.gov)